Nitrification and nitrous oxide production in the offshore waters of the Eastern Tropical South Pacific

Alyson E. Santoro[1]*, Carolyn Buchwald[2], Angela N. Knapp[3], William M. Berelson[4], Douglas G. Capone[5], Karen L. Casciotti[6]

[1]Department of Ecology, Evolution, and Marine Biology, University of California, Santa Barbara, California, USA; [2]Department of Oceanography, Dalhousie University, Halifax, Nova Scotia, Canada; [3]Earth, Ocean, and Atmospheric Science Department, Florida State University, Tallahassee, Florida, USA; [4]Department of Earth Sciences, University of Southern California, Los Angeles, California, USA; [5]Department of Biological Sciences, University of Southern California, Los Angeles, California, USA; [6]Department of Earth System Science, Stanford University, Stanford, CA, USA

*Corresponding author: Alyson E. Santoro (asantoro@ucsb.edu)

Key points:

- Depth-integrated ammonia oxidation rates are correlated with sinking particulate nitrogen flux, indicating substrate supply as a primary control of water column nitrification.
- Nitrous oxide (N_2O) is produced from ammonium (NH_4^+) in the water column, with an instantaneous N_2O yield from nitrification (N_2O-N/NO_3^-) lower than previous estimates.
- Higher than anticipated N_2O concentrations were measured in offshore waters, which may arise from local production, leading to large air-sea fluxes of N_2O.

Running head: *Nitrification in the offshore ETSP*

Abstract

Marine oxygen deficient zones (ODZs) are dynamic areas of microbial nitrogen cycling. Nitrification, the microbial oxidation of ammonia to nitrate, plays multiple roles in the biogeochemistry of these regions, including production of the greenhouse gas nitrous oxide (N_2O). We present here the results of two oceanographic cruises investigating nitrification, nitrifying microorganisms, and N_2O production and distribution from the offshore waters of the Eastern Tropical South Pacific (ETSP). On each cruise, high-resolution measurements of ammonium ($[NH_4^+]$), nitrite ($[NO_2^-]$), and N_2O were combined with ^{15}N tracer-based determination of ammonia oxidation, nitrite oxidation, nitrate reduction and N_2O production rates. Depth-integrated inventories of NH_4^+ and NO_2^- were positively correlated with one another, and with depth-integrated primary production. Depth-integrated ammonia oxidation rates were correlated with sinking particulate organic nitrogen flux but not with primary production; ammonia oxidation rates were undetectable in trap-collected sinking particulate material. Nitrite oxidation rates exceeded ammonia oxidation rates at most mesopelagic depths. We found positive correlations between archaeal *amoA* genes and ammonia oxidation rates and between *Nitrospina*-like 16S rRNA genes and nitrite oxidation rates. N_2O concentrations in the upper oxycline reached values of >140 nM, even at the western extent of the cruise track, supporting air-sea fluxes of up to 1.71 μmol m^{-2} d^{-1}. Our results suggest that a source of NO_2^- other than ammonia oxidation may fuel high rates of nitrite oxidation in the offshore ETSP and that air-sea fluxes of N_2O from this region may be higher than previously estimated.

Keywords

Ammonia oxidation, nitrite oxidation, nitrate reduction, nitrous oxide, oxygen deficient zones

1. Introduction

Marine oxygen deficient zones (ODZs) are dynamic areas of microbial nitrogen cycling. In the four major oceanic ODZs, oxygen (O_2) concentrations in the water column are low enough to allow the microbial nitrogen removal processes of denitrification and anaerobic ammonium oxidation (anammox) (Devol, 2008). Together these two processes set the fixed nitrogen inventory of the ocean by returning biologically fixed nitrogen back to N_2 gas. Nitrification, the microbial oxidation of ammonia (NH_3) to nitrite (NO_2^-) and ultimately nitrate (NO_3^-), plays an important role in linking nitrogen inputs and losses in ODZs because it produces the substrates necessary for denitrification and anammox (Lam *et al.*, 2007; Ward *et al.*, 2009).

Aside from its role as a link between sources and sinks in the nitrogen cycle, nitrification plays other important roles in marine biogeochemistry. First, nitrification may influence estimates of nitrate-driven 'new' production by providing a recycled source of NO_3^- within the euphotic zone (Dugdale and Goering, 1967). Second, ammonia oxidation, the first step of nitrification, evolves the long-lived greenhouse gas nitrous oxide (N_2O). N_2O production has been linked to the metabolism of both ammonia-oxidizing bacteria (AOB) (Goreau *et al.*, 1980) and ammonia-oxidizing archaea (AOA) (Löscher *et al.*, 2012; Santoro *et al.*, 2011). N_2O is correlated with apparent oxygen utilization (AOU), a measure of organic matter remineralization, and thus nitrogen remineralization, throughout the world's oceans, though with varying slopes (Nevison *et al.*, 2003). N_2O cycling is hypothesized to be dynamic at the fringes of ODZs, where N_2O may be both produced by ammonia oxidation and produced and consumed by denitrification (Babbin *et al.*, 2015; Cohen and Gordon, 1979; Ji *et al.*, 2015). The amount of N_2O cycling through each of these pathways, however, is poorly quantified as are the exact enzymatically and non-enzymatically catalyzed reactions leading to N_2O production during ammonia oxidation (Kozlowski *et al.*, 2016; Liu *et al.*, 2017). The fate of N_2O within ODZ waters has important implications for quantifying how much N_2O originating in the ODZ is eventually released to the atmosphere, where it contributes to both greenhouse warming and ozone depletion (Bianchi *et al.*, 2012; Martinez-Rey *et al.*, 2015; Yang *et al.*, in press).

The Eastern Tropical South Pacific (ETSP) is the second largest marine ODZ by area. While pioneering (Codispoti and Christensen, 1985; Lipschultz *et al.*, 1990; Ward *et al.*, 1989) and more recent (*e.g.*, (Bourbonnais *et al.*, 2015; Casciotti *et al.*, 2013; Kalvelage *et al.*, 2013; Lam *et al.*, 2009; Peng *et al.*, 2016)) field campaigns have brought attention to the dynamic nitrogen biogeochemistry in the ODZ core (from the Peruvian shelf out to approximately 85º W), less attention has been paid to offshore waters of the eastern Pacific, where low O_2, relatively high [NO_2^-], high N_2O waters impinge on the extremely oligotrophic waters of the south Pacific gyre. In these offshore waters, O_2 concentrations in most of the water column are higher than typically believed to permit water column denitrification, thought to initiate at 2.5 – 4.5 µmol L^{-1} (Bianchi *et al.*, 2012; Devol, 2008). These O_2 concentrations are low enough, however, to potentially influence the rate and efficiency of aerobic nitrogen cycling processes, such as nitrification (Bristow *et al.*, 2016), as well as support anaerobic nitrogen cycling processes within microenvironments on sinking particulate matter (Bianchi *et al.*, 2018). Low but non-zero O_2 concentrations may also influence the coupling of the two steps of nitrification (ammonia oxidation and nitrite oxidation), supporting a dynamic oxidation, reduction, re-oxidation loop with implications for the overall N and C stoichiometry of ODZs (Buchwald *et al.*, 2015; Granger and Wankel, 2016; Sigman *et al.*, 2005).

Recent studies have suggested that uncertainties in our ability to model and predict N_2O emissions from the ocean result from a poor understanding of the quantitative relationship between nitrification and N_2O production as a function of O_2 (Zamora *et al.*, 2012). This is further complicated by uncertainties in the mechanisms by which N_2O is produced during ammonia oxidation. It has been suggested that, because N_2O in AOA cultures may not form directly from an enzymatic reaction, its production should not be influenced by ambient oxygen concentration (Stieglmeier *et al.*, 2014). This is in direct contrast to empirical observations, however, which clearly show dependence of N_2O yield (the amount of N_2O-N produced for every mole of NO_2^- produced) on O_2 (Qin *et al.*, 2017). Indeed, recent experiments have shown that N_2O production in the ocean, where AOA are the dominant and often only ammonia oxidizers (Santoro *et al.*, 2010; Wuchter *et al.*, 2006), is tied to ammonia oxidation and increases at low O_2 (Ji *et al.*, 2015; Ji *et al.*, 2018; Trimmer *et al.*, 2016).

We present here the results of two oceanographic cruises investigating nitrification and nitrifying microorganisms in the offshore waters of the Eastern Tropical South Pacific (ETSP), extending from the continental shelf out to 100ºW. On each cruise, we determined rates of ammonia oxidation, nitrite oxidation, and euphotic zone nitrate reduction using ^{15}N tracers and quantified the abundance of nitrifying organisms (AOB, AOA, and nitrite-oxidizing bacteria, NOB) in the context of NO_2^-, NH_4^+, and N_2O distributions. We further quantified N_2O production from NH_4^+ and determined N_2O yield across environmental O_2 concentrations. Finally, we coupled contemporaneous estimates of air-sea gas exchange to N_2O concentration measurements to estimate the atmospheric flux of N_2O to the atmosphere.

2. Methods

2.1 Cruise track and hydrography

Sampling was conducted on two cruises to the ETSP in Feb-Mar 2010 ('Year 1') aboard the R/V *Atlantis* (cruise AT15-61) and Mar-Apr 2011 ('Year 2') aboard the R/V *Melville* (cruise MV1104). Both cruises were part of a larger project to quantify the impact of biological nitrogen fixation and carbon export in this region of the ocean (Berelson *et al.*, 2015; Haskell *et al.*, 2015; Knapp *et al.*, 2016). The cruise track in both years was a rectangular box, occupying six major stations numbered counterclockwise (Fig. 1). The southern transect extended along 20ºS from 80ºW to 100ºW (Stations (Stns.) 1-5) and the northern transect was along 10ºS, from approximately 82.5ºW to 100ºW (Stns. 7-11). In both years, hydrographic data were collected with using an SBE-9 profiling conductivity, temperature, depth (CTD) sensor package (SeaBird Electronics) additionally equipped with a fluorometer (Seapoint or WetLabs), transmissometer, a Clark-type electrode oxygen sensor (SBE 43, SeaBird), and photosynthetically active radiation sensor (Biospherical/Licor). CTD sensor data were processed using SeaSoft v7.2 (SeaBird) including application of the hysteresis and tau corrections for deep water oxygen measurements (Edwards *et al.*, 2010).

Discrete water samples were collected using Niskin bottle-type rosette sampler equipped with either (24) 10 L bottles or (12) 20 L Niskin bottles.

2.2 Dissolved nutrient analyses

Ammonium concentration ($[NH_4^+]$) was determined on-ship in unfiltered 50 mL seawater samples using *o*-phthaldialdehyde derivatization (Holmes *et al.*, 1999) and measurement on an Aquafluor 8000 handheld fluorometer (Turner Designs), with modifications as suggested

in (Taylor *et al.*, 2007). Nitrite concentration ([NO_2^-]) was determined on-ship in unfiltered 50 mL sample volumes using standard colorimetric methods (Strickland and Parsons, 1968). NH_4^+ standards (30 – 300 nM) were freshly prepared for each analysis in duplicate using deep water (> 500 m) from the same station, which consistently had a lower blank than ultrapure water. Samples for [NO_2- + NO_3-] were stored frozen and determined in the laboratory using vanadium reduction followed by chemilumenescence detection (Braman and Hendrix, 1989), and [NO_3-] was calculated by difference. Detection limits for [NH_4^+], [NO_2^-], and [NO_3^-] were 10 nM, and 100 nM for both [NO_2^-] and [NO_3^-] analyses.

2.3 Tracer-based rate measurements

2.3.1 Net primary production

Net primary production (NPP) was determined in deckboard bottle incubations in both years. In Year 1, for each depth, four 2 L polycarbonate bottles were filled directly from Niskin bottles from a pre-dawn CTD rosette cast and amended with stable isotope-labeled sodium bicarbonate ($NaH^{13}CO_3$) to a final concentration of 25 µM. A single bottle was filtered immediately after isotope addition to establish an initial (T_0) atom% ^{13}C of the particulate carbon for each depth. The remaining triplicate bottles were placed in surface seawater filled circulating incubators and shaded by different mesh size combinations of aluminet screening to simulate ambient light intensity. Incubations were carried out for ~24 h. All samples were filtered onto precombusted (5 h at 400˚C) 25 mm GF/F filters (Whatman), dried, and stored until analysis on an IsoPrime continuous flow isotope ratio mass spectrometer at the University of Southern California. In Year 2, NPP was determined with radiotracers (^{14}C) using established protocols from the Bermuda Atlantic Time-Series and were previously reported in (Knapp *et al.*, 2016).

2.3.2 Ammonia and nitrite oxidation rates

Ammonia and nitrite oxidation rates were determined using ^{15}N tracer additions (>98 atm% $^{15}NH_4Cl$ or $Na^{15}NO_2^-$, Cambridge Isotope Laboratories). As described below, incubation methods varied slightly between the first and second cruises.

In Year 1, rates were determined at four depths at all six stations, targeting the middle of the euphotic zone, the primary nitrite maximum, the base of the euphotic zone, and the upper oxycline. Incubations were conducted in 160 mL glass serum vials capped with 20 mm diameter Teflon-backed gray butyl septa (Microliter Analytical, 20-0040AS) and sealed with aluminum crimps. Bottles were filled from the Niskin sampling bottles using silicone tubing, allowing approximately three volumes of sample water to overflow the bottle prior to collection. Six serum bottles were filled and sealed from each incubation depth, spiked with ^{15}N tracer (100-200 nM $^{15}NH_4Cl$ or $Na^{15}NO_2^-$) using a plastic syringe, and incubated in flowing seawater incubators screened to mimic the *in situ* light environment (euphotic zone samples) or temperature controlled chambers (sub-euphotic zone). Duplicate bottles were sacrificed at timepoints of 0, 12, and 24 h from each incubation depth, 0.2 µm syringe-filtered into a 60 mL HDPE bottle, and frozen at -20ºC.

In Year 2, rates were determined at six depths at five stations between the middle of the euphotic zone and 500 m depth. Due to undetectable rates encountered in the Year 1 cruise at Stn 5 (see Results), no rates were determined at Stn 5 in Year 2. Incubations were conducted in 500 mL Tedlar bags (Restek) equipped with a septum injection port and three-way stopcocks for tracer addition and sampling, respectively. Bags were acid washed and

purged with N_2 between incubations. Duplicate incubation bags per treatment were filled from the Niskin bottles using silicone tubing, and ^{15}N tracer (200 nM $^{15}NH_4Cl$ or $Na^{15}NO_2$) was added via the septum injection port. As in the previous year, bags were incubated at as close to *in situ* light and temperature as possible. At timepoints of 0, 12, 24, and 36 h, 50 mL samples were drawn from each bag through the three-way sampling port using a 60 mL syringe while applying constant pressure to the incubation bag. At each timepoint, incubation water was 0.2 µm syringe filtered into a 60 mL HDPE bottle tripled rinsed with sample, and frozen at -20ºC. At the conclusion of the experiment, the volume remaining in the bag was drained into a graduated cylinder to calculate the initial seawater volume in the bag at the beginning of the experiment.

Frozen samples were transported to the laboratory, thawed, and prepared for $\delta^{15}N_{NO2+NO3}$ analysis using the 'denitrifier method' (Sigman *et al.*, 2001) and analyzed on a custom purge and trap system interfaced to a Thermo Delta Plus XP isotope ratio mass spectrometer (IRMS) (McIlvin and Casciotti, 2011). For nitrite oxidation rate samples, the added $^{15}NO_2^-$ tracer was removed using sulfamic acid addition and subsequent neutralization with NaOH (Granger *et al.*, 2006) prior to sample preparation and analysis. For 2010 samples, where only three timepoints were taken, rates were calculated using the linear fitting method of Dugdale and Goering (Dugdale and Goering, 1967). For 2011, where four timepoints were taken, rates were calculated using a least squares fitting approach that accounts for changes in $\delta^{15}N_{NO2+NO3}$ from co-occurring nitrate uptake (Santoro *et al.*, 2010).

2.3.3 Nitrate reduction rates

Nitrate reduction rates to nitrite were determined in Year 2 using $^{15}NO_3^-$ tracer additions (>98 atm% $Na^{15}NO_3$, Cambridge Isotope Laboratories). Because our focus was on the potential for NO_2^- production from assimilatory nitrate reduction by photoauthotrophs and subsequent leakage from cells (Lomas and Lipschultz, 2006), $^{15}NO_3$- incubations were only conducted in the euphotic zone (three depths) at the five stations where ammonia and nitrite oxidation rates were made. Tedlar incubation bags were prepared and filled as above, and 200 or 400 nM (final concentration) of $Na^{15}NO_3$ was added to each bag using a plastic syringe. Timepoints were sampled and preserved as for the nitrification rate incubations above. In the laboratory, samples were prepared for $\delta^{15}N_{NO2}$ determination using the 'azide method' (McIlvin and Altabet, 2005). Special sample handling and preparation were required to analyze $\delta^{15}N_{NO2}$ at the low concentrations encountered on the cruise, and to reduce the possibility of $^{15}NO_3^-$ contamination of the laboratory. Briefly, thawed samples with sufficient NO_2^- (*i.e.* in samples where [NO_2-] was > 0.5 µM) were aliquoted into 20 mL glass vials at the volume necessary to achieve 5 nmol NO_2^- analyte. Sargasso Sea surface water was then added to a final volume of 10 mL. When [NO_2^-] was < 0.5 µM, 10 mL of sample was added to each headspace vial and the $NaNO_2^-$ isotope standard N7373 was added as carrier to a final amount of 5 nmol. Finally, 10 µmol of KNO_3- was added to each sample to dilute the initial $^{15}NO_3$- tracer and samples were purged with ultra-high purity N_2 for 30 min. Following azide conversion to N_2O, samples and standards (N23, N7373, and N10219; (Casciotti *et al.*, 2007) were analyzed by IRMS and rates were calculated as described above.

2.3.4 Light inhibition experiments

Light inhibition experiments were conducted in Year 2 to test the effect of sunlight on ammonia oxidation, nitrite oxidation, and nitrate reduction. These incubations were conducted at the two shallowest incubation depths, approximating the 1% and 10% light

depths at Stns. 7, 9, and 11. For these experiments, one set of duplicate incubation bottles for each rate type was incubated at ambient light and the other in the dark. Tracer addition, subsampling, analysis, and rate calculations were as described above for each individual rate type.

2.3.5 Particle-associated ammonia oxidation rates

Ammonia oxidation occurring in association with sinking particulate organic matter was measured in both years (n = 8 experiments). Sinking particulate organic matter was captured in drifting surface-tethered particle interceptor sediment traps ('PIT' traps) as described previously (Haskell *et al.*, 2013). Each trap had 12 collection tubes that contained a funnel and 50 mL centrifuge tube (BD Falcon) at the base of each tube. In Year 1, particle-associated rates were measured at Stations 7 and 9 using material from a single collection tube from traps deployed at 200 m depth. On recovery of the trap, the trapping solution (a concentrated NaCl brine) was decanted and particulate matter was resuspended in 15 mL of 0.2 µm-filtered seawater obtained from 200 m depth at the respective station. 5 mL of this particle slurry was distributed to each of three 160 mL glass serum vials. Each vial was filled with additional filtered seawater to a volume of 100 mL and spiked with $^{15}NH_4Cl$ to a final concentration of 100 nM [NH_4^+]. Three bottles containing only filtered seawater served as a negative control for ammonia oxidation that was not particle-associated. Bottles were sampled for δ^{15}NOx analysis after 24 h as described above for water column ammonia oxidation rates.

In Year 2, particle-associated rates were measured at Stations 1, 7, and 11 using particulate material from traps deployed at both 100 m and 200 m depths. Due to concerns that the trap brine fluid used in the prior year could be negatively impacting particle-associated microbial communities, centrifuge tubes designated for collection of incubation particles contained only filtered seawater as a trap solution. On recovery of the trap, the seawater in the centrifuge collection tube was decanted to the conical portion of the tube and particles were resuspended in 10 mL of filtered seawater from the particle collection depth. A cutoff 5 mL pipette was used to distribute 3 mL of particle slurry into each of three 160 mL serum vials. Each vial was filled with additional filtered seawater to a volume of 100 mL and spiked with $^{15}NH_4Cl$ to a final concentration of 400-600 nM [NH_4^+]. Three bottles containing only filtered seawater served as a negative control.

Particles were filtered at the conclusion of the experiment onto 0.2 µm Supor filters (Pall) for DNA extraction and analysis, thus no material was available for mass determination. As such, the mass of particulate carbon added to each incubation was estimated from the average areal particulate carbon flux (Haskell *et al.*, 2013).

2.4 Dissolved N_2O concentration and production rates

2.4.1 N_2O concentration

Samples for [N_2O] analysis at 24 depths per station were drawn directly from the rosette after dissolved oxygen samples were collected but before other sample collection, using silicone tubing directed into a 160 mL glass serum bottle. The tubing was placed at the bottom of the serum bottle and water was allowed to overflow the bottle for approximately 30 seconds (approximately 3 volumes of the sample bottle). The tubing was then slowly withdrawn, and 1 mL of water was removed from the bottle to allow for expansion of the liquid during storage.

The sample was preserved with the addition of 100 µL of saturated mercuric chloride solution, then capped with a gray butyl stopper (MicroLiter Analytical, 20-0025) and sealed with an aluminum crimp. Samples were stored at room temperature in the dark until analysis.

N_2O concentration measurements were performed on an IRMS using a custom-built automated purge and trap system (McIlvin and Casciotti, 2010). Dissolved N_2O concentrations were determined by comparison of mass/charge (*m*/*z*) = 44 peak area against analyses of known amounts of N_2O (1-10 nmol) and the volume of sample analyzed (153.8 ± 0.5 mL). N_2O saturation was calculated relative to water in equilibrium with the atmosphere (Weiss and Price, 1980), assuming a 'modern' atmospheric concentration of 322 ppb, the modern tropospheric concentration for the Southern Hemisphere at the time of the cruises (2010-2011) (Combined N_2O data obtained from the NOAA/ESRL Global Monitoring Division, American Samoa station: ftp://ftp.cmdl.noaa.gov/hats/n2o/combined/HATS_global_N2O.txt). Standard deviations for [N_2O] are based on analyses of replicate samples. A total of 605 concentration measurements are presented here. Although $\delta^{15}N_{N2O}$, $\delta^{18}O_{N2O}$ and isotopomers of N_2O ('site preference') were determined in concert with the concentration measurement, a full treatment of those data is outside the scope of the present manuscript.

2.4.2 N_2O production rates

Nitrous oxide production from ammonia oxidation was determined in incubations with added $^{15}NH_4Cl$ at Stns. 1, 9, and 11 in both years. In Year 1, N_2O production rates were determined at the same four depths as nitrification rates; in Year 2, N_2O production rates were determined at three of the six depths where ammonia oxidation rates were also measured: the primary nitrite maximum, just below the primary nitrite maximum, and the top of the oxycline. Incubations were conducted in 160 mL glass serum vials capped with 20 mm diameter Teflon-backed gray butyl septa (Microliter Analytical, 20-0040AS) and sealed with aluminum crimps. Bottles were filled from the Niskin bottles using silicone tubing, allowing approximately three volumes of sample water to overflow the bottle prior to collection. Six serum bottles were filled to overflowing and sealed from each incubation depth, spiked with ^{15}N tracer (100-200 nM $^{15}NH_4Cl$) using a plastic syringe, and incubated in temperature-controlled chambers as above. Duplicate bottles were killed at timepoints of 0, 12, 24 h from each incubation depth by the addition of 100 µL of saturated $HgCl_2$. In Year 2, similar procedures were followed except that experiments were conducted in triplicate and an additional timepoint was added (36 h). N_2O isotope measurements were determined by isotope ratio mass spectrometry and calibrated against pulses of N_2O reference gas analyzed just prior to elution of each sample (McIlvin and Casciotti, 2010). The reference gas has been calibrated against AIR ($\delta^{15}N$) and VSMOW ($\delta^{18}O$) reference scales by S. Toyoda (Tokyo Institute of Technology) (McIlvin and Casciotti, 2010).

N_2O production rates from NH_4^+ ($R_{N2O\text{-}N}$ in nmol N_2O-N d^{-1}) were calculated using the slope of the timecourse [$^{45}N_2O$] and [$^{46}N_2O$], where *F* is the fraction of ^{15}N in the substrate (NH_4^+) pool:

$$R_{N2O-N} = \frac{1}{F}\left(\frac{d[^{45}N2O]}{dt} + 2\frac{d[^{46}N2O]}{dt} \times \frac{1}{F}\right)$$

This formulation follows prior work (Ji et al., 2015; Trimmer et al., 2016; Ji et al., 2018) accounting for the production of singly and doubly labeled N_2O from NH_4^+. The 1/*F* terms account for production of unlabeled N_2O via the same pathways. The probability of $^{46}N_2O$

production is proportional to $1/F^2$, thus the extra factor of $1/F$ is needed in that term relative to production of $^{45}N_2O$.

2.5 Quantitative PCR (qPCR)

Quantitative PCR (qPCR) assays were conducted using group-specific assays for the thaumarchaeal ammonia monooxygenase subunit a (*amoA*) gene for the 'shallow' water column ecotype A (WCA) and 'deep' water column ecotype B (WCB) (Mosier and Francis, 2011) with TaqMan Environmental Mastermix (Life Technologies) chemistry on a CFX96 qPCR machine (Bio-Rad, Inc., Hercules, CA) as described previously (Santoro *et al.*, 2017). Detection limits for TaqMan assays were 1 copy mL^{-1} or better. All samples were run in triplicate against a standard curve spanning approximately 10^1 - 10^5 templates, run in duplicate. Plasmids containing cloned inserts of the target gene (TOPO pCR4 vector, Invitrogen or pGem vector, Promega) were used as standards. Standards were linearized with the restriction enzyme NotI or ScaI (New England Biolabs), purified (DNeasy, Qiagen), quantified by fluorometry (Quanti-T HS reagent, Invitrogen), and stored at -80ºC. Fresh standard dilutions were made from frozen stocks for each day of analysis. All qPCR runs were setup using an epMotion 5075 automated liquid handling system (Eppendorf) to minimize between-run variability. Ammonia oxidizing bacteria (AOB; Year 1 only) and *Nitrospina*-like 16S rRNA genes were quantified using primers (Mincer *et al.*, 2007) and protocols (Santoro *et al.*, 2010) described previously with SYBR Green chemistry. We verified (in silico) that this assay captures recently-described uncultivated *Nitrospina* from low oxygen waters (Sun *et al.*, 2019).

3. Results

3.1 Hydrography and nutrient distributions

3.1.1 Temperature, oxygen, and chlorophyll

There were strong east-west gradients in all hydrographic parameters along both the northern and southern transects (Table S1, Fig. 1). On the southern transect along 20ºS (Stns. 1-5), sea surface temperature (SST) ranged from 20.6 to 23.4ºC in 2010, with mixed layer depths from 28-68 m. The northern transect along 10ºS (Stns. 7-11) had higher SSTs (23.8 – 26.5ºC) and shallower mixed layer depths. In general SSTs were higher in 2011 (on average 0.7 ºC higher), particularly at Stn 7, where SST was 2.6ºC higher.

We used an arbitrary definition of 10 µmol kg^{-1} $[O_2]$ to define the boundaries of the ODZ for between-station and between-year comparisons. The ODZ was thicker on the northern transect, ranging from 205 m thick at Stn 7 to 539 m thick at Stn 9. On the southern transect, an ODZ was only present at Stn 1. On the eastern edge of the cruise track, oxygen concentrations were near the ~1 µmol kg^{-1} detection limit of the SBE43 sensor at Stn 9, 11, and 13. The ODZ was thicker in Year 2, but did not extend as far offshore. For example, the ODZ at St 11 was 467 m thick in Year 1, but 662 m thick in year 2.

There were pronounced deep chlorophyll maxima (DCM) at all stations, as deep as 137 m at Stn 5 (Table S1, Fig. 2). Chl *a* profiles at Station 11 contained a secondary Chl *a* maximum within the ODZ (Fig. 2c). In both years, the northern transect along 10ºS (Stn 7, 9, and 11) was characterized by higher primary production, higher surface Chl *a*, and higher depth integrated Chl *a* than the southern transect (Table S1).

3.1.2 [NH_4^+] and [NO_2^-]

Ammonium concentrations displayed typical distributions for stratified water columns, with low but occasionally detectible [NH_4^+] in surface waters increasing to a subsurface maximum just below the deep chlorophyll maximum, and concentrations below detection limits at deeper depths (Fig. 2). Particularly elevated shallow [NH_4^+] was observed at Stn 11 in both years, where [NH_4^+] reached concentrations of up to 660 nM in surface waters. Concentrations within the deep ammonium maximum ranged from 13 nM at the offshore Stn 5, to 2 µM at Stn 11. When [NH_4^+] data from both years are plotted together against density, the profiles are nearly identical (Fig. S1).

A primary nitrite maximum (PNM) was present at all stations just below the ammonium maximum (Fig. 2), ranging in concentration from 0.38 µM at Stn 5 (in year 1) to nearly 3 µM at Stn 11 (also in year 1). Coincident with detectible [NH_4^+] in surface waters, measurable NO_2^- was present in surface waters at Stn 7 and 9 in year 1 and Stns 7, 9, and 11 in year 2. A deeper, secondary nitrite maximum (SNM) was detectable within the ODZ at Stns 1, 9, and 11 in 2010, ranging from 0.31 µM at Stn 1 to 2.1 µM at Stn 11. The ODZ did not extend as far west in 2011, and an SNM was only present at Stn 11 and 13 in that year. As with [NH_4^+], when [NO_2^-] data from both years are plotted against density, profiles are very similar (Fig. S2) with the exception of a much larger PNM at Stn 11 in year 1 versus year 2 (3.0 µM versus 1.3 µM).

Depth-integrated inventories of NH_4^+ and NO_2^- between the surface and 200 m were correlated with one another (Fig. S3a; Spearman's *rho* = 0.82, *p* = 0.003), and with depth-integrated primary production (*rho* = 0.70, *p* = 0.02), with the highest inventories of both at the station with highest primary production (Stn 11).

3.2 Rate measurements

3.2.1 Ammonia oxidation and nitrite oxidation rates

In general, ammonia and nitrite oxidation rates were low to undetectable in the euphotic zone, highest in a subsurface maximum just below the PNM, and decreased with depth. In both years, rates of both processes were higher along 10ºS than 20ºS, and were highest in the east, closer to the coast (Fig. 3). Given the higher density of sampling, we specifically discuss here only the rates from year 2. Rates from both years are given in Table S2.

Ammonia oxidation was detectible in the deep euphotic zone at Stns 9, 11, and 13 in both years, with rates of 0.9 – 5.8 nmol L^{-1} d^{-1} (Fig. 3, Table S2). Mean ammonia oxidation rates within the subsurface rate maximum ranged from 1.7 $\pm$ 1.4 nmol L^{-1} d^{-1} at Stn 3 to 50.8 $\pm$ 20.0 nmol L^{-1} d^{-1} at Stn 11. Nitrite oxidation rate profiles had a similar shape to the ammonia oxidation rate profiles, however nitrite oxidation was more frequently detected in the euphotic zone, with rates above detection limits at the 1% light depth at all stations except Stn 7.

There was a marked difference in magnitude between ammonia oxidation and nitrite oxidation rates in both years, with nitrite oxidation rates being much greater at a given depth. Nitrite oxidation rates within the subsurface maximum ranged from 15.0 $\pm$ 0.3 nmol L^{-1} d^{-1} at Stn 9 to 57.1 nmol L^{-1} d^{-1} at Stn 13. The largest offsets between ammonia oxidation and nitrite oxidation occurred near the base of the euphotic zone and at the lowest oxygen

concentrations. At Stn 13, nitrite oxidation rates continued to increase with depth into the ODZ, reaching rates of 65.0 ± 0.4 nmol L^{-1} d^{-1} at 100 m.

To investigate the factors controlling nitrification rates in the upper water column, we categorized rate samples as originating from the euphotic zone, PNM, or upper oxycline after (Peng *et al.*, 2016). Neither ammonia oxidation nor nitrite oxidation rates were correlated with substrate concentration ([NH_4^+] or [NO_2^-]) or oxygen concentration (data not shown) within these categories. We further compared depth-integrated nitrification rates in the upper mesopelagic (to 300 m depth) with primary production in the overlying euphotic zone and sinking particulate organic nitrogen (PON) flux from sediment traps for both years. Depth-integrated ammonia oxidation rates in the mesopelagic were not correlated with depth-integrated primary production in the overlying euphotic zone, either in individual years or when data from both years are combined (*rho* = 0.50, *p* = 0.10). Depth integrated ammonia oxidation rates were, however, correlated with absolute sinking PON flux at 200 m (*rho* = 0.82, *p* = 0.003; Fig. S4).

Ammonia oxidation rates in deeper waters (1000 - 2000 m depth) were determined at a subset of stations in both years (*n* = 10, Table 1). Rates were low but detectable at these depths at all stations, and ranged from 0.10 nmol L^{-1} d^{-1} to 0.88 nmol L^{-1} d^{-1}. In all cases, ammonia oxidation rates were lower at the deepest depth at each station. At the only station to include deep rate measurements in both years (Stn 7), rates were not different between years (student's *t*-test, *p* < 0.0001).

3.3.2 Nitrate reduction rates

Rates of nitrate reduction to nitrite were highest in the upper euphotic zone, ranging from averages of 366 nmol L^{-1} d^{-1} at Stn 13 to 109 nmol L^{-1} d^{-1} at Stn 11 (Table 2). Nitrate reduction in the euphotic zone occurred at higher rates than either ammonia or nitrite oxidation. Deeper in the euphotic zone, nitrate reduction to nitrite was below detection limits at the 1% light depth (the PNM) and the upper oxycline, with the exception of the depth of the PNM at Stn 13, where nitrate reduction was 9.7 nM d^{-1}. There was no relationship between nitrate reduction rate and primary production at an individual depth, or with depth-integrated primary production by station.

3.3.3 Light inhibition experiments

Rates of ammonia and nitrite oxidation were both higher in dark bottles compared to light bottles at the 1% light depth at Stn 11 (Fig. 4a,b). We observed a slight increase in relatively low nitrite oxidation rates in the light at both the 1% and 10% light depths at Stn 7 and 9, with a significant difference at the 1% light depth at Stn 7. Nitrate reduction rates were always higher in the light (Fig. 4c).

3.3.4 Particle-associated ammonia oxidation rates

Ammonia oxidation rates were below the detection limit in particle samples from both Stn 7 and Stn 11 in Year 1. Similarly, in Year 2, ammonia oxidation was below detection limits in 4 out of 6 incubations (Table S3). Low rates of ammonia oxidation were detected on particles from the two most productive stations, Stn 1 from the 200 m trap depth (0.09 ± 0.1 nmol mg^{-1} d^{-1}) and Stn 11 from the 200 m trap depth (0.18 ± 0.08 nmol mg^{-1} d^{-1}).

3.4 Nitrous oxide distribution and production

3.4.1. *N_2O distribution*

General patterns in N_2O distribution were consistent between years, with higher N_2O concentrations on the northern transect at any given longitude, and relatively small horizontal gradients in N_2O concentration (Fig. 5a,b). N_2O was slightly supersaturated in surface waters at all stations in both years. Below the surface, the shapes of the N_2O profiles were qualitatively similar in both years, with some notable exceptions. Evidence of N_2O loss processes were present in profiles from Stn 9 and Stn 11 on the northern transect, particularly in Year 2, where N_2O concentrations decreased beginning at the upper oxycline to midwater minima of 18.7 nM (Stn 11) between 300 and 400 m depth forming a 'bite' in the N_2O profile. Deep water concentrations (sigmaT > 30) were not different between years, with the exception of Stn 5, where deep N_2O concentrations were elevated by 2-3 nM in 2011 relative to 2010 (Fig. S5).

A notable feature in the N_2O dataset along 10°S was a sharp peak of very high N_2O concentration in the upper oxycline, even at the western extent of the cruise track, reaching 145 nM (sigma T = 26.56, depth = 90 m) at Stn 9 in Year 2 and 122 nM (sigma T 26.89, depth = 150 m) at Stn 7 in Year 1. In both cases, these peaks in N_2O concentration occurred just above local minima in N_2O, and were higher than observed closer to the ODZ core.

3.4.2 *Rates of N_2O production from ammonia oxidation*

N_2O production from ammonia was determined using $^{15}NH_4Cl$ tracer incubations at the three stations nearest the ODZ (Stns 1, 9, and 11; Table S4). In Year 1, N_2O production ranged from below the detection limit at Stn 1 to 83 pmol L^{-1} d^{-1} at Stn 11 at the top of the oxycline. In Year 2, N_2O production rates ranged from below detection limits to 156 pmol L^{-1} d^{-1} in the upper oxycline, again at Stn 11.

N_2O production rates were used in conjunction with measured ammonia oxidation rates (see above) to calculate the N_2O yield from ammonia oxidation (N_2O-N/mol NO_3^- produced, expressed as a percentage). N_2O yields ranged from 0.02% in the euphotic zone at station 1 to 2.93% at the top of the ODZ at station 11. The highest N_2O yields were observed in samples with < 10 µM O_2 (Fig. 6).

3.5 Abundance of nitrifying microorganisms

Profiles of *amoA* genes from ammonia-oxidizing archaea and 16S rRNA genes from *Nitrospina*-like nitrite-oxidizing bacteria were similar in shape to nitrification rate profiles: low in the euphotic zone, a maximum at the base of the euphotic zone, and decreasing with depth below (Fig. S6). Abundances of both archaeal *amoA* and *Nitrospina* 16S rRNA genes were slightly lower in Year 1 (Table S5), though sampling resolution was much lower in that year. Archaeal *amoA* abundance was highest at Stn 11, reaching concentrations of 2.0×10^5 *amoA* genes mL^{-1} at 200 m depth. Combining all samples from both years, total archaeal *amoA* genes were correlated with *Nitrospina*-like 16S rRNA genes and best described by an exponential relationship ($n = 54$, $R^2 = 0.81$, $p < 0.0001$ on $\log_{10}$ transformed data, Fig. S7).

Particulate samples obtained from sediment traps in Year 2 were also screened for the presence of nitrifying organisms (n = 6). Five of six samples were below detection limits for archaeal *amoA*, and all samples were below detection limits for *Nitrospina*. The exception was the 100 m trap from station 7, which contained 1550 *amoA* genes mg^{-1} particle (Table S5).

Ecotype-specific qPCR assays were used to quantify the shallow (WCA) and deep (WCB) clades of ammonia-oxidizing archaea for Year 2 samples. WCA-like *amoA* genes were more abundant in samples shallower than 200 m, while WCB-like *amoA* genes were more abundant below. The transition from a WCA-dominated community to a WCB-dominated community was sharp, with the vast majority of samples containing >90% of one ecotype or the other (Table S5).

There was no significant relationship between total *amoA* genes and ammonia oxidation rates. There was, however, a positive correlation between WCA *amoA* genes and ammonia oxidation rates (R^2 = 0.61, p < 0.0001; Fig. 7a). *Nitrospina*-like 16S rRNA genes were also positively correlated with nitrite oxidation rates (R^2 = 0.40, p < 0.001; Fig. 7b).

4. Discussion

4.1 Nitrification in the context of upper ocean organic matter remineralization

Our data show the direct connection between sinking particulate organic nitrogen (PON) flux and ammonia oxidation rates in the upper ocean. This relationship has been explored previously by comparison of nitrification rate profiles and organic matter flux attenuation profiles, which both display a power law relationship with depth (Martin *et al.*, 1987; Ward, 2008; Ward and Zafiriou, 1988). Previous work has found a close correspondence between power law exponents (attenuation coefficients, or '*b*' values) calculated from fitting a power law function to both particulate organic carbon (POC) flux profiles and nitrification rates (Newell *et al.*, 2011; Peng *et al.*, 2015; Smith *et al.*, 2015), though previous studies have not been able to make contemporaneous measurements on the same cruise. Here, as previously reported for the equatorial Pacific (Santoro *et al.*, 2017), we found a correlation between direct measurements of PON flux attenuation and depth-integrated nitrification rates, suggesting that even in oxygen poor regions of the ocean, the primary control on depth-integrated nitrification rates is substrate supply delivered by sinking particulate matter.

Though there was a correlation between sinking PON flux and nitrification rates, we found little evidence for nitrification occurring on particles either in ^{15}N-based rate measurements or in molecular assays designed to target AOA and NOB. Particle-associated ammonia oxidation rates were low to undetectable, AOA were detected in only one sediment trap sample, and *Nitrospina*-like organisms not detected in any. This is consistent with previous findings indicating that thaumarchaea are enriched in the free-living fraction of size-fractionated metagenomes (Fuchsman *et al.*, 2017; Ganesh *et al.*, 2014). Thus, it appears that sinking particles serve as sites of ammonification and/or urea release, but that the nitrification process occurs among free-living microorganisms in the water column. As [NH_4^+] is less than 10 nM at the depths of highest ammonia and nitrite oxidation rates (except at Stn. 13), ammonium regeneration from particles and oxidation must be closely coupled (Ploug and Bergkvist, 2015). Narrow zones of particle processing have been identified at density interfaces in the water column, where slow particle sinking rates lead to zones of

intense remineralization (Prairie *et al.*, 2017). Interestingly, we find an intense zone of nitrification just below the euphotic zone, which may indicate one such region (Fig. 3).

Depth-integrated nitrification rates were not correlated with primary production, yet we found that the euphotic zone ammonium and nitrite inventories were linearly related to primary production. While this general trend has been observed previously (Raimbault *et al.*, 2008; Santoro *et al.*, 2013), this quantitative relationship between depth-integrated inventories has only been reported once (Brzezinski, 1988) as extensive shipboard [NH_4^+] profiles are relatively rare. This observation provides support for the hypothesis that the source of NO_2^- in the PNM originates from ammonia oxidation, as ammonia oxidation provides a direct link between the inventories of NH_4^+ and NO_2^-. The factors limiting nitrite oxidation in the PNM that allow such high accumulations of NO_2^- (here up to 3 μM) still remain to be elucidated. A recent modeling study suggested that the depth distribution of [NH_4^+] and [NO_2^-] around the PNM could be explained by differences in the cell sizes and energy yields of ammonia and nitrite oxidizers, predicting an [NH_4^+]:[NO_2^-] of about 1:10 at the PNM (Zakem *et al.*, 2018). Here, we find [NH_4^+]:[NO_2^-] at the PNM much lower, $\leq$1:100, suggesting additional, poorly understood biological or physical factors (such as grazing or mixing) that raise the effective subsistence concentration of NO_2^- for NOB.

A somewhat surprising finding in our study was the relatively high [NH_4^+] (up to 660 nM) and [NO_2^-] (160 nM) in surface waters. The ocean is the largest natural source of NH_3 to the atmosphere (Johnson *et al.*, 2008; Paulot *et al.*, 2015); our data are consistent with global biogeochemical models (Paulot *et al.*, 2015) indicating the ETSP is a large potential source of NH_x to the atmosphere. High model-derived NH_x flux from this region has previously been interpreted to derive from iron limitation, and contemporaneous measurements of iron limitation on our cruises did find evidence for iron limitation of N_2 fixation (Dekaezemacker *et al.*, 2013) at the same locations where we observed high [NH_4^+]. An alternative explanation (Paulot *et al.*, 2015) suggests that high surface water [NH_4^+] originates from photolysis of DON. In either case, ammonia oxidation rates were below detection in the upper euphotic zone at these stations, which would allow NH_4^+ to accumulate. In contrast, rates of nitrite oxidation in the upper euphotic zone are slightly higher in the light (Fig. 4), suggesting that the NO_2^- supporting this process must originate from something other than ammonia oxidation, such as nitrate reduction by phytoplankton or photolysis of NO_3^- (Zafiriou and True, 1979). Our results from the light-dark experiments support previous work showing that ammonia oxidation rates are lower in the light (Horak *et al.*, 2018; Smith *et al.*, 2014a), though our experimental design cannot resolve whether this effect is due to competition with phytoplankton for NH_4^+ or direct photoinhibition.

4.2 Apparent decoupling between ammonia and nitrite oxidation

We frequently observed large differences between the magnitude of ammonia oxidation and nitrite oxidation rates (Fig. 3). Large offsets between these two processes are unexpected in oxic water columns, as the only source of NO_2^- to support nitrite oxidation should be from ammonia oxidation, thus constraining the nitrite oxidation rate to the ammonia oxidation rate. Yet, such offsets have been reported previously in coastal ODZs (Bristow *et al.*, 2017; Buchwald *et al.*, 2015; Ganesh *et al.*, 2015; Kitzinger *et al.*, 2020; Lipschultz *et al.*, 1990), and the causes of such offsets are infrequently discussed. Here we explore several hypotheses that could explain these observations.

If the observed rate differences are methodological artifacts, they could result from either an underestimation of the ammonia oxidation rate or an overestimation of the nitrite oxidation rate. An underestimation of ammonia oxidation could be due to isotope dilution of the added $^{15}NH_4^+$ by newly produced NH_4^+, as has been reported for ammonium uptake measurements (Glibert *et al.*, 1982). If an underestimation of ammonia oxidation due to isotope dilution is the cause, we would expect to see the biggest offsets between ammonia oxidation and nitrite oxidation at the depths of the highest ammonia oxidation rates. We did observe a correlation between the ammonia oxidation rate at a given depth and the magnitude of the ammonia oxidation and nitrite oxidation rate difference at the same depth (r = 0.51, p < 0.01; Fig. S8a), providing partial support for this idea. Another potential cause of underestimation of ammonia oxidation rates is a greater sensitivity of ammonia-oxidizing organisms to bottle incubation conditions than NOB.

The alternative explanation for the observed offset between ammonia oxidation and nitrite oxidation is that we are overestimating the nitrite oxidation rate, either due to stimulation by oxygen introduced in the handling process or substrate stimulation of NO_2^- limited organisms. There is a very strong correlation between the ammonia and nitrite oxidation rate offset and the magnitude of the nitrite oxidation rate (r = 0.94, p < 0.0001; Fig. S8b), suggesting that the observed offsets are controlled primarily by variation in nitrite oxidation. While the largest offset was observed at 1 µmol kg^{-1} O_2, large offsets were also observed at 160 – 200 µmol kg^{-1} O_2, arguing against a role for O_2 stimulation in controlling the offset. Timecourse measurements of $^{15}N/^{14}N$ in the tracer incubations were highly linear (data not shown), perhaps providing evidence against oxygen contamination. Further, nitrite oxidation in ODZs has been shown to have a half-saturation constant (K_m) of < 1 µM for O_2 (Bristow *et al.*, 2016), below most of the *in situ* concentrations observed here. Given the extremely low [NO_2^-] at most of the incubation depths, stimulation of nitrite oxidation by the addition of $^{15}NO_2^-$ tracer is certainly a possibility. K_m values for NO_2^- for marine NOB are few, but the data that do exist indicate values in the 20-30 µM range (Jacob *et al.*, 2017).

A final but intriguing possibility is that the offsets between ammonia and nitrite oxidation rates in bottle experiments are real and accurately reflect a stoichiometric decoupling of the two processes in the water column. Nitrate reduction within anoxic zones in sinking aggregates may provide an additional source of NO_2- for nitrite oxidation in the water column. Modeling suggests that nitrate reduction rates could be high even in oxic water columns (Bianchi *et al.*, 2018), and recent geochemical and metagenomic data suggest an enrichment of nitrate-reducing activity in particle-associated over free-living environments (Fuchsman *et al.*, 2017; Ganesh *et al.*, 2015). Unfortunately, the nitrate reduction rate measurements conducted as part of this study were limited to the upper water column and cannot be used to answer this question.

4.3 Insights into nitrification from organismal distributions

Our data suggest that specific clades of AOA contribute differentially to ammonia oxidation in the water column. The abundance of the shallow ecotype of marine AOA (the 'WCA' clade), which contains the cultivated AOA *Candidatus* Nitrosopelagicus brevis (Santoro *et al.*, 2015), was strongly correlated with ammonia oxidation rates with a very similar slope to that found by (Smith *et al.*, 2014b) in Monterey Bay (Fig. 7a).

There is a close, but non-linear, coupling of AOA and NOB in water column. The mean ratio of NOB to AOA was 0.49 when samples containing <10 genes mL^{-1} are removed. This is much higher than recently reported for the Gulf of Mexico (Kitzinger *et al.*, 2020), but is

similar to the ratio of NOB:AOB reported for nitrifying sequencing batch reactors (Dytczak *et al.*, 2008). It has been suggested that deviations from this ratio resulting in high NOB:AOB ratios may result from coupling between denitrification and nitrification, as present in activated granular sludge (Winkler *et al.*, 2015). In our data, however, deviations from this ratio were not clearly tied to ambient oxygen concentration (Fig. S7). It should be noted that the NOB:AOA ratio we calculate here does not account for other potential NOB, such as *Nitrospira spp*. or *Nitrococcus spp*., but *Nitrospina* have been shown to be the most abundant both within and along the margins of other low oxygen regions in the Pacific (Beman *et al.*, 2013; Ganesh *et al.*, 2015; Sun *et al.*, 2019).

The qPCR data may also provide some insight into the offsets observed between ammonia oxidation and nitrite oxidation – the correlation between nitrite oxidation rates and *Nitrospina* gene copies suggests that the nitrite oxidation rates are accurate and reflect the abundance of NOB in the water column, thus implying that the observed offsets between ammonia oxidation and nitrite oxidation are real.

4.4 Contribution of ammonia oxidation to N_2O distributions in the offshore ETSP

In both years, N_2O production from NH_4^+ was detectible from at least one depth at all stations where measurements were made (i.e., Stns. 1, 9, and 11). Thus, despite arguments that AOA are incapable of N_2O production, there is clear production of N_2O from $^{15}NH_4^+$, presumably carried out by AOAs in these samples, consistent with previous marine observations (Ji *et al.*, 2015; Ji *et al.*, 2018; Yoshida *et al.*, 1989). We observed both $^{45}N_2O$ and $^{46}N_2O$ production in our incubations, indicating production of both singly and doubly labeled N_2O from NH_4^+. At most depths, production of singly labeled N_2O exceeded production of doubly labeled N_2O. Due to the high atom% ^{15}N labeling of the NH_4^+ pool, singly labeled N_2O is most likely to occur through a hybrid mechanism, while the doubly labeled N_2O could arise from a NH_4^+ oxidation pathway. Whether enzymatic or not, this strongly suggests that at least some N_2O production is occurring within the cell envelope of ammonia oxidizers and results from a combination of pathways as originally proposed for the AOA (Santoro *et al.*, 2011), and consistent with recent laboratory experiments (Jung *et al.*, 2019).

The N_2O yield from nitrification is an important parameter for modeling N_2O production in the ocean, and is a large source of uncertainty in global biogeochemical models. N_2O yield from nitrification has been estimated from geochemical measurements based on the relationship between N_2O supersaturation and AOU (Nevison *et al.*, 2003). This relationship breaks down, however, in low oxygen regions of the ocean due to the combined and potentially opposing effects of nitrification and denitrification at low O_2, where there may be increased N_2O yield from nitrification, as well as denitrification, but also potential consumption of N_2O due to microbial denitrification. Experimental data are needed to separate the contributions of these processes in order to effectively model microbial N_2O production in low oxygen regions (Martinez-Rey *et al.*, 2015; Suntharalingam *et al.*, 2000). We report here N_2O yields (mol N_2O-N/mol NO_3^-) from nitrification of 0.003 – 2.93%, which are similar to, but somewhat lower than, N_2O yields from ammonia oxidation in the ETSP ODZ core (Ji *et al.*, 2015; Ji *et al.*, 2018), where N_2O yields as high as 3.14% were reported. Our values are about 50 times lower than those reported in classic culture experiments with ammonia-oxidizing bacteria grown at high density with high substrate concentrations (Goreau *et al.*, 1980), but very similar to results from more field-relevant conditions 0.051% and 0.055% (220 and 22 µM O_2) for *Nitrosomonas marina* (Frame and Casciotti, 2010) and marine ammonia-oxidizing archaea (0.004 – 0.11%)(Qin *et al.*, 2017; Santoro *et al.*, 2011).

Nevison (Nevison *et al.*, 2003) modeled N_2O yield as a function of oxygen using available laboratory culture data at the time (Goreau *et al.*, 1980) with the simple function:

$$\%\ N_2O\ \text{yield (mol } N_2O/\text{mol } NO_3^- * 100) = a_1 / O_2 + a_2 \qquad [1]$$

with best-fit values of $a_1 = 0.20$ and $a_2 = -0.0004$. Note that (Nevison *et al.*, 2003) expressed N_2O yield as mol N_2O/mol NO_3- (*not* mol N_2O-N as reported above for culture comparisons) and O_2 in units of µmol L^{-1}, thus the coefficients a_1 and a_2 in Eq. [1] apply to yields and O_2 expressed in those units. Recently, Ji and coworkers (Ji *et al.*, 2018) updated this relationship using N_2O yields from ^{15}N tracer experiments in the core ETNP and ETSP ODZs. We combined our field data together with the data of Ji et al. 2018 and recent data from cultures of marine ammonia-oxidizing archaea grown under different oxygen conditions (Qin et al., 2017, Santoro, *unpublished*) to further refine this relationship. Fitting Eq. 1 (again, with units of mol N_2O/mol NO_3-) to those data, we obtain coefficients (± 95% CI) of $a_1 = 0.11 \pm 0.05$ and $a_2 = 0.077 \pm 0.07$ (Fig. 6). It should be noted, however, that there is considerable scatter in the field data at low [O_2], and that a major assumption of least-squares fitting methods is that there is no error in the independent variable (*i.e.*, [O_2]). Given the imprecision of standard oxygen electrodes at low [O_2], we suggest that future experiments should focus on N_2O yield measurements in the critical window of O_2 <10 µmol kg^{-1}, and conduct continuous O_2 monitoring throughout the incubation rather than relying on CTD measured O_2 values as we (and others) have done. Our data appear to support previous field (Bristow *et al.*, 2016; Ji *et al.*, 2015) and laboratory (Qin *et al.*, 2017) experiments that suggest nitrification can proceed at concentrations of O_2 near 1 µmol L^{-1}, lower than the 2-4 µmol L^{-1} used in previous modeling efforts (Babbin *et al.*, 2015).

4.5 Source of N_2O in offshore waters and implications for atmospheric N_2O flux

We found that N_2O accumulates to high concentrations (>140 nM) in the ETSP outside of the ODZ core. In the ODZ core, previous measurements attributed high rates of N_2O production to both nitrification (Ji *et al.*, 2015; Peng *et al.*, 2016) and denitrification (Babbin *et al.*, 2015; Farias *et al.*, 2009). N_2O maxima above the ODZ over the continental shelf (70.70ºW) in the ETSP were 80-86 nM (Farias *et al.*, 2009; Peng *et al.*, 2016); here, we measured N_2O concentrations up to 122 nM as far offshore as 100º W (Stn 7) and 137 nM at 90º W (Stn 9), concentrations typically associated with highly productive coastal waters and episodic upwelling events (Arevalo-Martínez *et al.*, 2015; Bourbonnais *et al.*, 2017; Farías *et al.*, 2015). The steep N_2O gradients at the base of the mixed layer may also contribute to higher atmospheric N_2O fluxes than previously estimated. Indeed, based on a range of air-sea gas exchange parameterizations, atmospheric N_2O fluxes averaged along 10ºS are estimated at 1.30 – 1.71 µmol m^{-2} d^{-1} (Table 3), 1.7 – 2.2 times higher than previously estimated in this offshore region (Nevison *et al.*, 1995), but much lower than atmospheric fluxes measured closer to the Peruvian and Chilean coast (12.7 – 30.7 µmol m^{-2} d^{-1} (Farias *et al.*, 2009), 459 – 1825 µmol m^{-2} d^{-1} (Arevalo-Martínez *et al.*, 2015)).

The source of the high N_2O at the base of the euphotic zone at 90º and 100º W is puzzling. It is possible that the observed N_2O is due to lateral advection from the ODZ, though N_2O concentrations further east at 82.5º W are lower (< 95 nM at the N_2O max at Stn 11), and elevated N_2O concentrations are not associated with T-S anomalies (data not shown). Using measured ammonia oxidation rates and the N_2O yield relationship derived above, we estimate an N_2O production rate from ammonia oxidation of 0.08 nmol L^{-1} d^{-1} at the depth of the N_2O maximum, and 0.12 nmol L^{-1} d^{-1} at the ammonia oxidation rate maximum, leading to

a residence time of over three years if ammonia oxidation is the only source of N_2O. Assuming a conservative vertical diffusivity of 0.7 cm^2 s^{-1} (Yeung *et al.*, 2015), the timescale for diffusion over the upper 100 m of the water column is on the order of 4.5 years. Thus, it is possible that these high concentrations result from a low but constant input of N_2O from nitrification that is not quickly removed by physical processes. Given the potential for reductive NO_2- production suggested by our tracer experiments, there is also the possibility of reductive N_2O production from microbial denitrification. Further investigation of physical transport of N_2O from the ODZs combined with isotopic analysis of the N_2O in these offshore waters should improve our understanding of the processes contributing to the observed N_2O distributions.

5. Conclusions

Combining measures of surface primary production, particle export, and subsurface nitrogen transformations reinforced the close connections between the mesopelagic nitrogen cycle and euphotic zone processes. Nitrogen incorporated into biomass during primary production sets the amount of particulate organic nitrogen available for remineralization in the lower euphotic zone, controlling the inventories of both [NH_4^+] and [NO_2^-] that accumulate there. Sinking particulate nitrogen flux exiting the euphotic zone, in turn, controls substrate availability to the mesopelagic nitrifying community below. Together, our molecular and geochemical data point to a dynamic nitrogen cycle in low oxygen areas of the ocean offshore of those typically investigated in ODZ studies, with the potential for previously unrecognized coupling of oxidative and reductive processes and greenhouse gas production. We provide additional data to support the growing body of evidence that ammonia oxidation in the ocean is directly linked to N_2O production. Our results highlight the need for additional refinement of the nitrification-N_2O yield parameterization and for higher resolution measurements of N_2O to resolve transport of N_2O both into and out of coastal ODZs.

6. Acknowledgments and Data Availability Statement

We thank the captains and crew of both the R/V *Atlantis* and R/V *Melville* for their invaluable help during the cruises. Technical support from Troy Gunderson, Matt Tiahlo, Nick Rollins, Matt McIlvin, and Matt Forbes was critical to the data reported here. Scientific discussions with Masha Prokopenko, William Haskell, Nicholas Nidzieko, Simon Yang and Bonnie Chang greatly improved the manuscript, as did manuscript comments from Barbara Bayer. Funding for the cruises was provided by United States National Science Foundation awards OCE-0850905 to ANK, DGC, and WMB; OCE-0961098 to KLC. Additional support for AES was provided through a Woods Hole Oceanographic Institution Postdoctoral Scholar Fellowship and a Sloan Foundation Early Career Award in Ocean Sciences. All datasets reported in this manuscript have been deposited in the United States Biological and Chemical Oceanography Data Management Office repository in association with project number 555516 (https://www.bco-dmo.org/project/555516). [*Author note: BCO-DMO currently has an ~8-10 week processing time. Datasets were submitted on 27 May 2020.*]

Table List

Figure List

Supplemental Table List

Supplemental Figure List

Tables

Table 1. Ammonia oxidation rates measured using $^{15}NH_4^+$ in deep waters of the Eastern Tropical South Pacific.

Year	Station	Depth (m)	Rate (nM d^{-1})	SE (nM d-1)
2010	5	1000	0.55	0.04
		2000	0.10	0.01
	7	1000	0.88	0.07
		2000	0.14	0.02
	9	1000	0.79	0.53
		2000	0.20	0.02
2011	7	1000	0.58	0.44
		2000	0.12	0.001
	13	1000	0.55	0.02
		1500	0.19	0.07

Table 2. Rates of nitrate (NO_3^-) reduction to nitrite (NO_2^-) measured using $^{15}NO_3^-$ tracer additions on the 2011 cruise. (BDL = below detection limit)

Station	Depth (m)	NO_3^- reduction rate (nM d^{-1})	SE rate (nM d^{-1})
7	30	261.2	63.5
7	85	0.1	0.0
7	140	BDL	
9	30	166.3	60.4
9	55	BDL	
9	80	0.0	0.0
11	14	108.8	49.6
11	55	1.5	0.2
11	70	BDL	
13	20	125.0	0.2
13	40	9.6	0.2
13	60	366.1	21.6

Table 3. Sea-to-air fluxes of N_2O in the Eastern Tropical South Pacific using data from the 2010 cruise. Fluxes were determined using gas transfer velocities calculated using both wind-speed based parameterizations (Ho *et al.*, 2006; Wanninkhof, 1992) and mixed-layer ^{222}Rn deficits, all as reported in (Yeung *et al.*, 2015).

Station	Mixed layer excess N_2O (µmol m^{-3})	Atmospheric N_2O flux (µmol m^{-2} d^{-1})		
		Wind-W92	Wind-H06	^{222}Rn-deficit
1	0.438	0.96	0.79	0.66
3	0.148	0.44	0.36	0.34
5	0.037	0.15	0.12	0.04
	0.037	0.13	0.11	0.09
7	0.490	1.67	1.37	1.32
	0.490	1.81	1.52	1.52
9	0.161	0.58	0.47	0.45
11	1.07	2.78	2.25	1.93
10ºS transect average		1.71 ± 0.90	1.40 ± 0.73	1.30 ± 0.62
20ºS transect average		0.42 ± 0.39	0.34 ± 0.32	0.28 ± 0.28

Figures

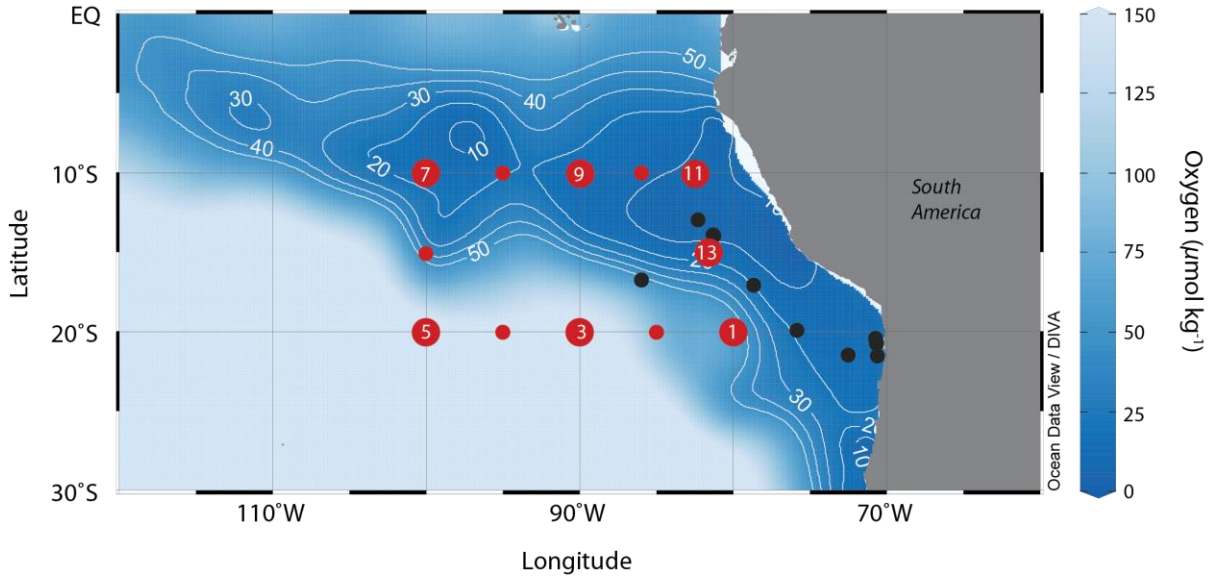

Figure 1. Map of the cruise track overlaid on dissolved oxygen concentration at the 200 m isobath (shown in both colorscale and contours). Large red dots indicate process study stations where rate measurements were conducted for the present study. Black dots indicate cruise track from (Ji *et al.*, 2015) and (Peng *et al.*, 2016). Oxygen data are monthly climatological means for March (1955-2012) from the World Ocean Atlas 1.00 degree gridded data product plotted in Ocean Data View v. 4.7.3 using the DIVA gridding algorithm with default settings.

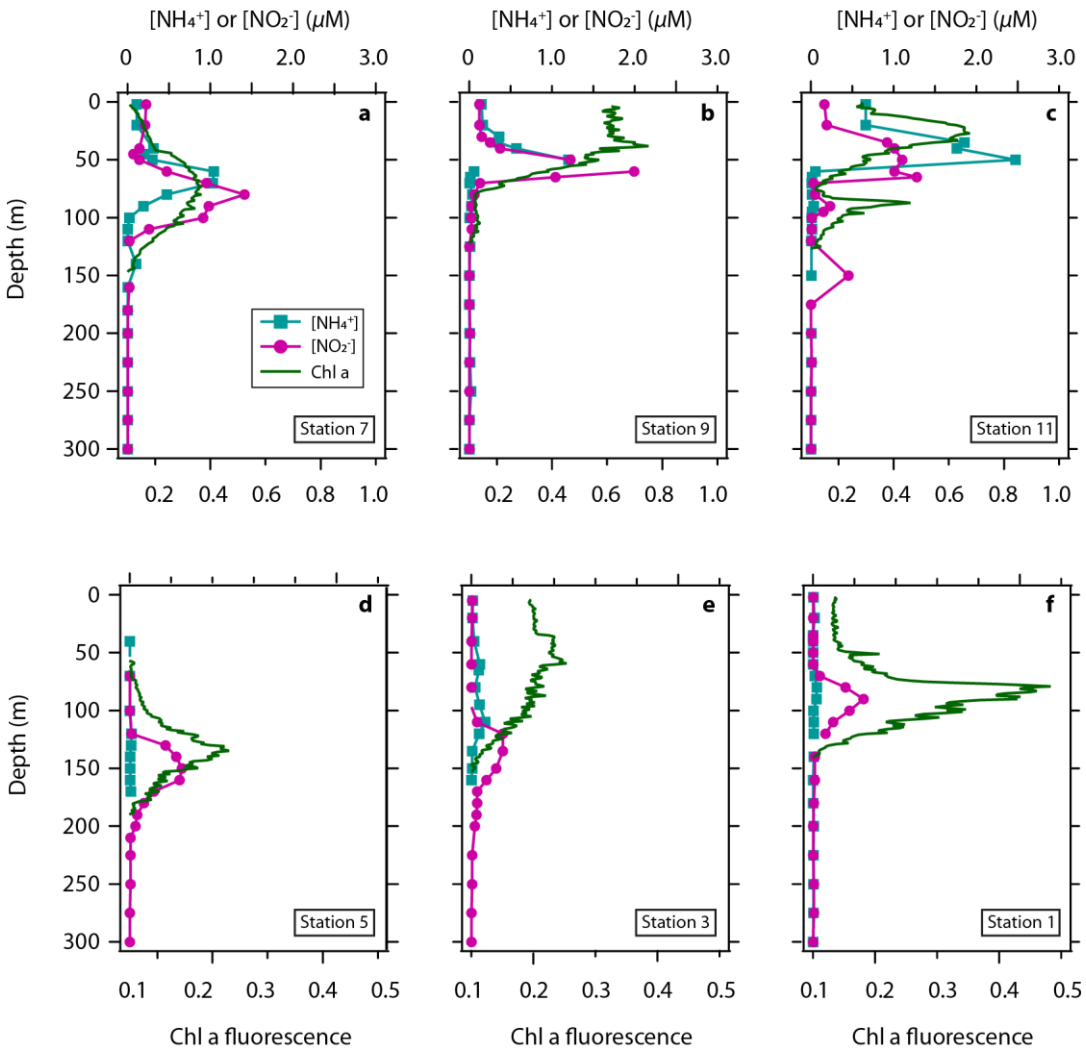

Figure 2. Profiles of ammonium ($[NH_4^+]$), nitrite ($[NO_2^-]$), and chlorophyll a fluorescence (Chl a) in the upper water column for the 2011 cruise along 10ºS: (a) Stn 7, (b) Stn 9, (c) Stn11; and 20ºS: (d) Stn 5, (e) Stn 3 (f) Stn1. Note the change in fluorescence scale between rows.

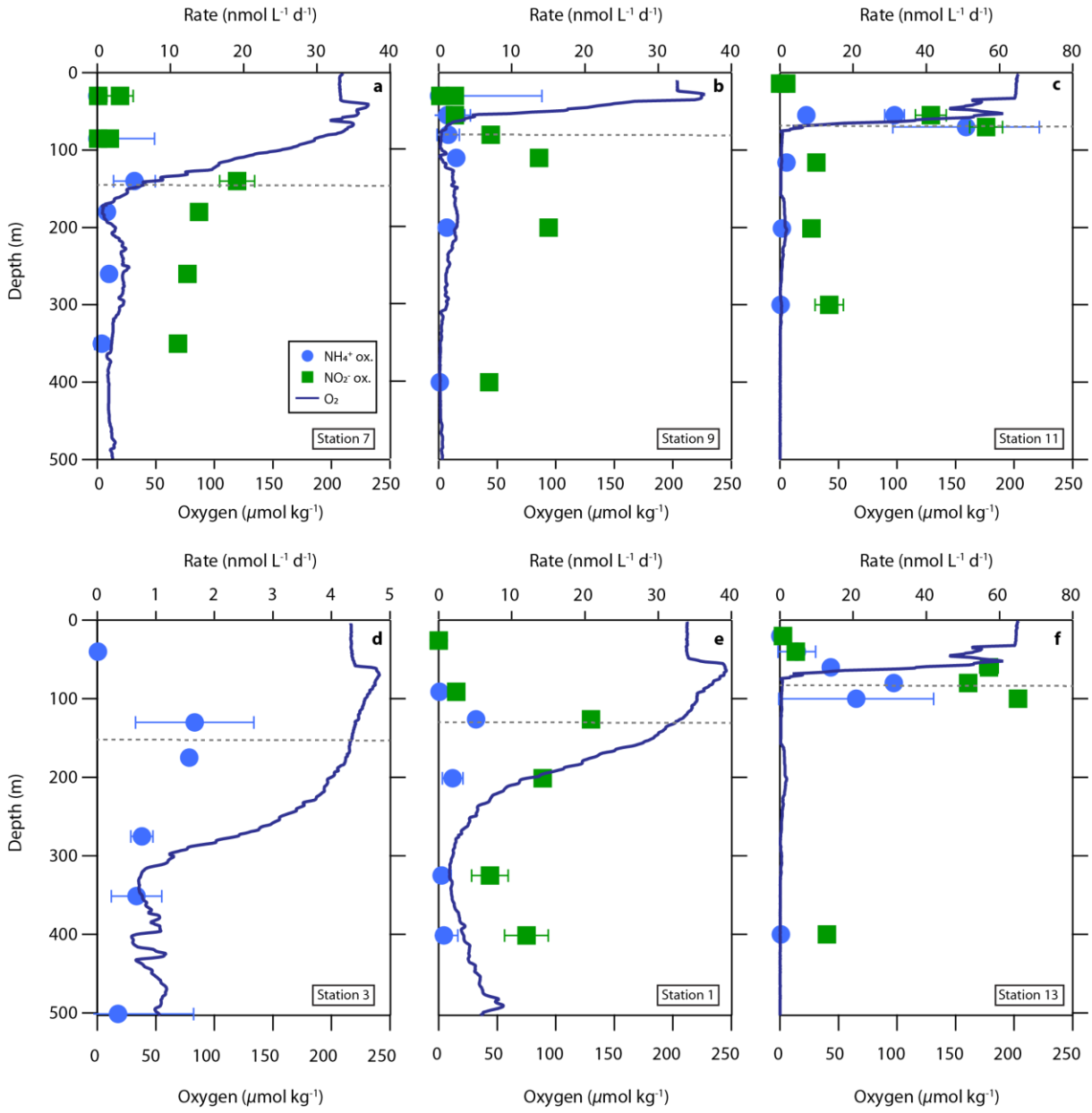

948
949
950 **Figure 3**. **Measured nitrite oxidation rates exceed ammonia oxidation rates in the**
951 **offshore ETSP**. Ammonia oxidation rate (NH_4^+ ox., blue circles), nitrite oxidation rate (NO_2^-
952 ox., green squares), and dissolved oxygen (dark blue line) along 10ºS: (a) Stn 7, (b) Stn 9,
953 (c) Stn11; and 20ºS: (d) Stn 3, (e) Stn 1 (f) Stn13. Depth of the euphotic zone is indicated by
954 the dashed line, calculated as 10% of the chlorophyll fluorescence maximum after correcting
955 for sensor background (Owens *et al.*, 2015). Note panel order differs from Fig. 2.
956

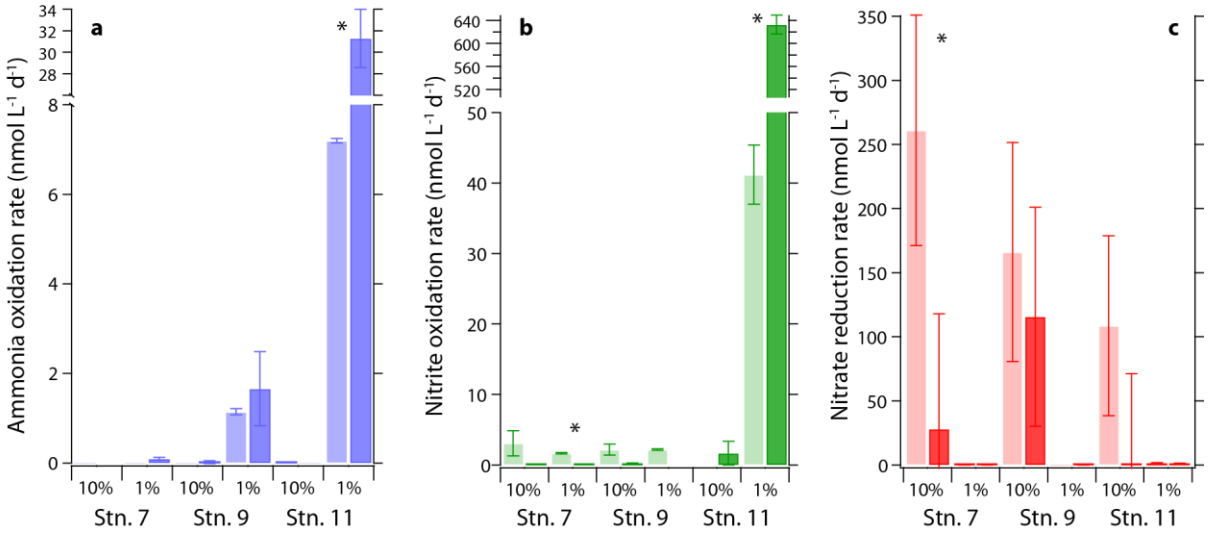

Figure 4. **Ammonia and nitrite oxidation rates are higher in the dark**. Rates of (a) ammonia oxidation, (b) nitrite oxidation, and (c) nitrate reduction measured in light (light bars) and dark (dark bars) incubations at Stns. 7, 9, and 11 during the 2011 cruise. Incubations were conducted with water collected from the depth of 10% surface irradiance and 1% surface irradiance at each station. Significant differences between the light and dark bottles at $p < 0.05$ are indicated with an asterisk.

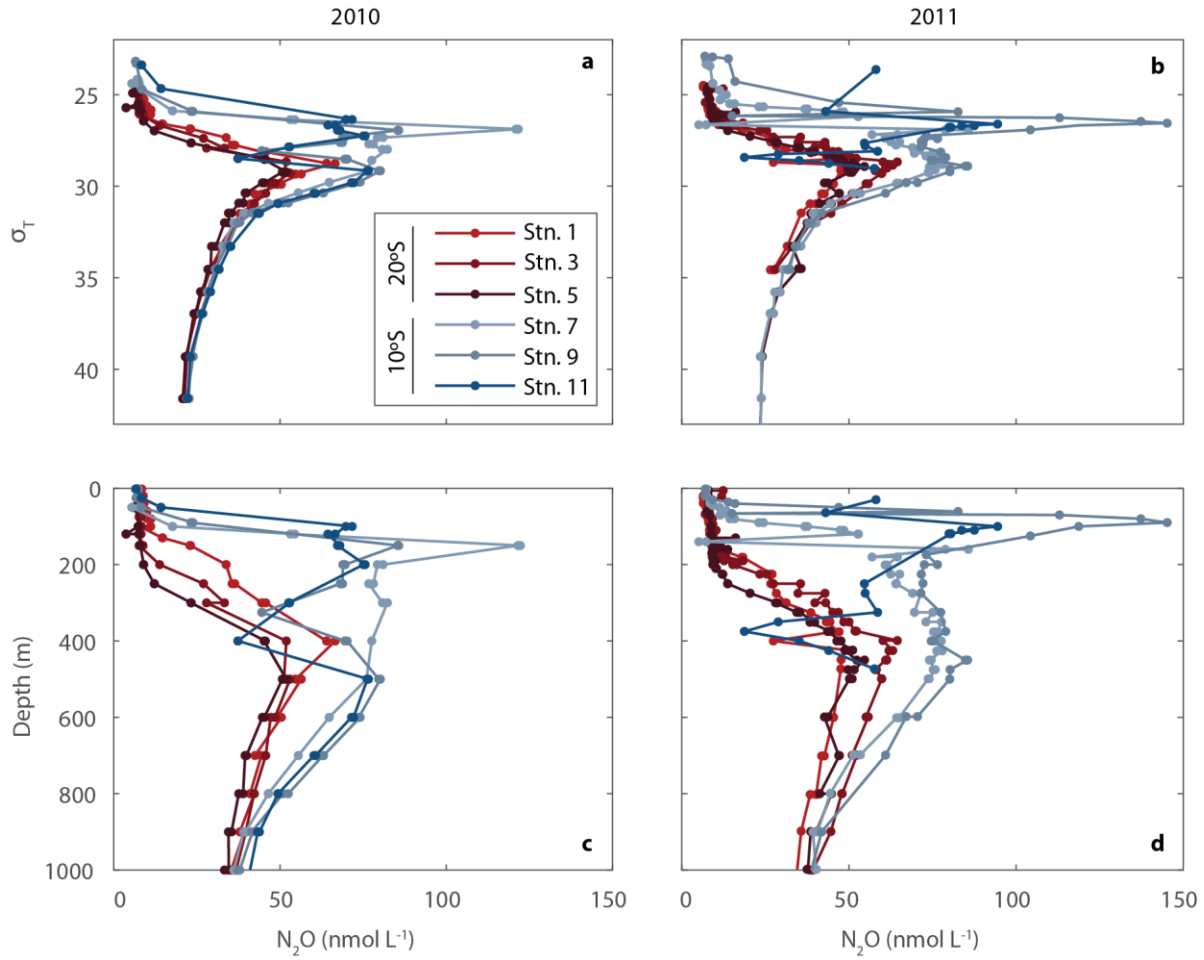

968
969
970 **Figure 5**. **Nitrous oxide (N_2O) concentrations in the water column of the offshore ETSP.**
971 Data are shown plotted against density (σ_T, panels **a**, **b**) and depth (panels **c**, **d**) in Year 1
972 (2010, left column) and Year 2 (2011, right column).
973
974
975

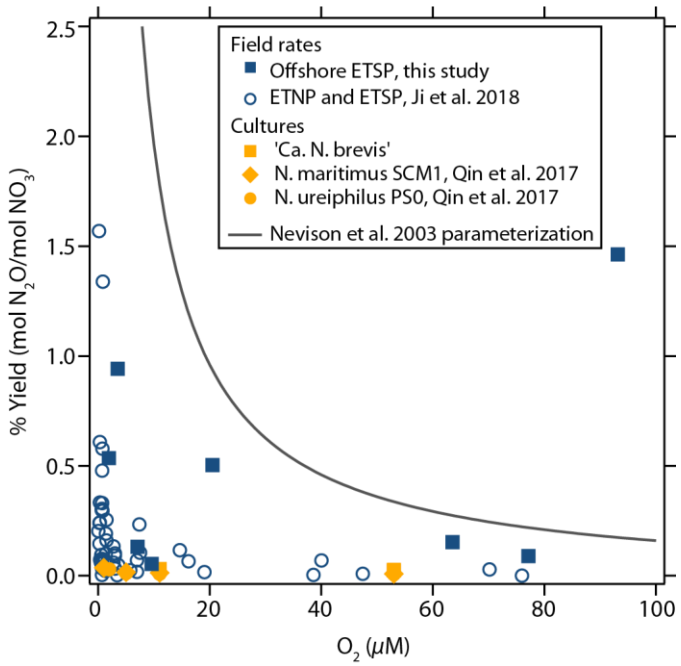

Figure 6. Nitrous oxide (N_2O) yield from ammonia oxidation in low oxygen water columns and cultures of ammonia-oxidizing archaea (orange symbols). The black line is the relationship fit by (Nevison *et al.*, 2003) to the culture data of (Goreau *et al.*, 1980) from ammonia-oxidizing bacteria. Consistent with other recent studies (Ji *et al.*, 2015; Ji *et al.*, 2018), we find a considerably lower instantaneous yield. Fitting Eq. [1] gives $a_1 = 0.11 \pm 0.05$ and $a_2 = 0.077 \pm 0.07$ (curve not shown); note that percent yield data are plotted here as mol N_2O/mol NO_3^- and O_2 in units of µmol L^{-1} for consistency with (Nevison *et al.*, 2003) . Samples with $O_2 < 0.05$ µmol L^{-1} were removed for fitting.

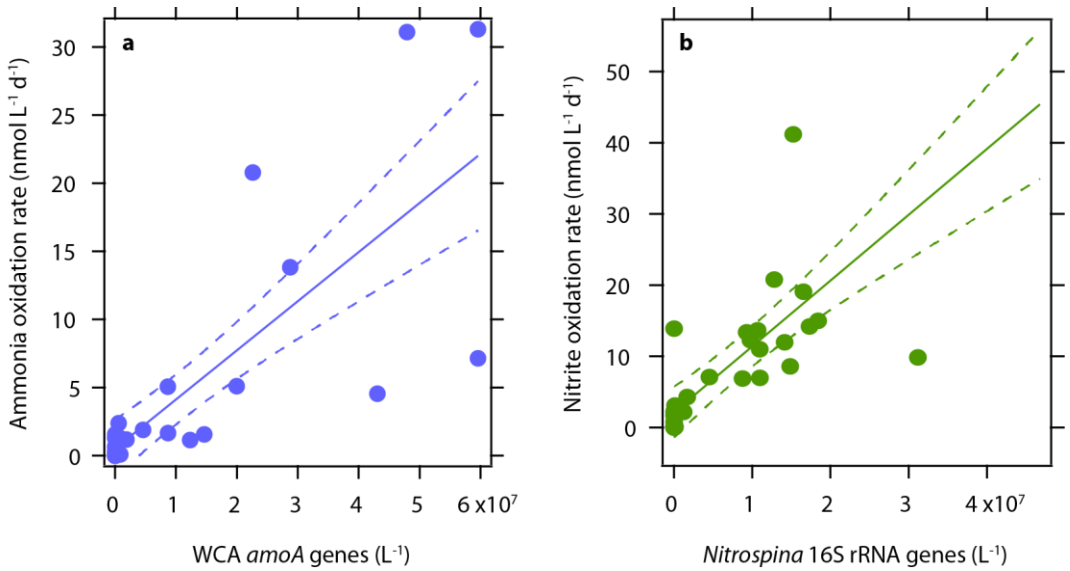

Figure 7. **Abundance of nitrifying organisms is correlated with the reactions they catalyze**. (a) Ammonia oxidation rate versus thaumarchaeal *amoA* gene abundance from the water column A (WCA) ecotype (slope = 3.61e-7, R^2 = 0.61, p < 0.0001) and (b) nitrite oxidation versus *Nitrospina*-like 16S rRNA gene abundance (slope = 6.89e-7, R^2 = 0.40, p < 0.001).

References

Arevalo-Martínez, D. L., A. Kock, C. Löscher, R. A. Schmitz, and H. W. Bange (2015), Massive nitrous oxide emissions from the tropical South Pacific Ocean, *Nat Geosci*, *8*(7), 530.

Babbin, A. R., D. Bianchi, A. Jayakumar, and B. B. Ward (2015), Rapid nitrous oxide cycling in the suboxic ocean, *Science*, *348*(6239), 1127-1129.

Beman, J. M., J. L. Shih, and B. N. Popp (2013), Nitrite oxidation in the upper water column and oxygen minimum zone of the eastern tropical North Pacific Ocean, *ISME J*, *7*(11), 2192-2205.

Berelson, W., W. Haskell, M. Prokopenko, A. Knapp, D. Hammond, N. Rollins, and D. Capone (2015), Biogenic particle flux and benthic remineralization in The Eastern Tropical South Pacific, *Deep Sea Res. I*, *99*, 23-34.

Bianchi, D., J. P. Dunne, J. L. Sarmiento, and E. D. Galbraith (2012), Data - based estimates of suboxia, denitrification, and N2O production in the ocean and their sensitivities to dissolved O2, *Global Biogeochemical Cycles*, *26*(2).

Bianchi, D., T. S. Weber, R. Kiko, and C. Deutsch (2018), Global niche of marine anaerobic metabolisms expanded by particle microenvironments, *Nat Geosci*, *11*(4), 263.

Bourbonnais, A., M. A. Altabet, C. N. Charoenpong, J. Larkum, H. Hu, H. W. Bange, and L. Stramma (2015), N - loss isotope effects in the Peru oxygen minimum zone studied using a mesoscale eddy as a natural tracer experiment, *Global Biogeochemical Cycles*, *29*(6), 793-811.

Bourbonnais, A., R. T. Letscher, H. W. Bange, V. Echevin, J. Larkum, J. Mohn, N. Yoshida, and M. A. Altabet (2017), N2O production and consumption from stable isotopic and concentration data in the Peruvian coastal upwelling system, *Global Biogeochemical Cycles*, *31*(4), 678-698.

Braman, R. S., and S. A. Hendrix (1989), Nanogram nitrite and nitrate determination in environmental and biological materials by vanadium (III) reduction with chemiluminescence detection, *Anal. Chem.*, *61*(24), 2715-2718.

Bristow, L. A., T. Dalsgaard, L. Tiano, D. B. Mills, A. D. Bertagnolli, J. J. Wright, S. J. Hallam, O. Ulloa, D. E. Canfield, and N. P. Revsbech (2016), Ammonium and nitrite oxidation at nanomolar oxygen concentrations in oxygen minimum zone waters, *Proceedings of the National Academy of Sciences*, *113*(38), 10601-10606.

Bristow, L. A., C. M. Callbeck, M. Larsen, M. A. Altabet, J. Dekaezemacker, M. Forth, M. Gauns, R. N. Glud, M. M. Kuypers, and G. Lavik (2017), N 2 production rates limited by nitrite availability in the Bay of Bengal oxygen minimum zone, *Nat Geosci*, *10*(1), 24.

Brzezinski, M. A. (1988), Vertical-Distribution of Ammonium in Stratified Oligotrophic Waters, *Limnol. Oceanogr.*, *33*(5), 1176-1182.

Buchwald, C., A. E. Santoro, R. H. Stanley, and K. L. Casciotti (2015), Nitrogen cycling in the secondary nitrite maximum of the eastern tropical North Pacific off Costa Rica, *Global Biogeochemical Cycles*, *29*(12), 2061-2081.

Casciotti, K. L., C. Buchwald, and M. McIlvin (2013), Implications of nitrate and nitrite isotopic measurements for the mechanisms of nitrogen cycling in the Peru oxygen deficient zone, *Deep Sea Res. I*, *80*, 78-93.

1044 Casciotti, K. L., J. K. Bohlke, M. R. McIlvin, S. J. Mroczkowski, and J. E. Hannon (2007),
1045 Oxygen isotopes in nitrite: Analysis, calibration, and equilibration, *Anal. Chem.*,
1046 *79*(6), 2427-2436.
1047 Codispoti, L., and J. Christensen (1985), Nitrification, denitrification and nitrous oxide
1048 cycling in the eastern tropical South Pacific Ocean, *Mar. Chem.*, *16*(4), 277-300.
1049 Cohen, Y., and L. Gordon (1979), Nitrous oxide production in the ocean, *J. Geophys. Res.*,
1050 *84*, 347-353.
1051 Dekaezemacker, J., S. Bonnet, O. Grosso, T. Moutin, M. Bressac, and D. Capone (2013),
1052 Evidence of active dinitrogen fixation in surface waters of the eastern tropical South
1053 Pacific during El Niño and La Niña events and evaluation of its potential nutrient
1054 controls, *Global Biogeochemical Cycles*, *27*(3), 768-779.
1055 Devol, A. H. (2008), Denitrification including Anammox, in *Nitrogen in the Marine*
1056 *Environment*, edited by D. G. Capone, D. A. Bronk, M. R. Mulholland and E. J.
1057 Carpenter, pp. 263-301, Academic Press.
1058 Dugdale, R. C., and J. J. Goering (1967), Uptake of new and regenerated forms of nitrogen in
1059 primary productivity, *Limnol. Oceanogr.*, *12*(2), 196-206.
1060 Dytczak, M. A., K. L. Londry, and J. A. Oleszkiewicz (2008), Activated sludge operational
1061 regime has significant impact on the type of nitrifying community and its nitrification
1062 rates, *Water research*, *42*(8-9), 2320-2328.
1063 Edwards, B., D. Murphy, C. Janzen, and N. Larson (2010), Calibration, response, and
1064 hysteresis in deep-sea dissolved oxygen measurements, *Journal of Atmospheric and*
1065 *Oceanic Technology*, *27*, 920-931.
1066 Farias, L., M. Castro-Gonzalez, M. Cornejo, J. Charpentier, J. Faundez, N. Boontanon, and N.
1067 Yoshida (2009), Denitrification and nitrous oxide cycling within the upper oxycline of
1068 the eastern tropical South Pacific oxygen minimum zone, *Limnol. Oceanogr*, *54*, 132-
1069 144.
1070 Farías, L., V. Besoain, and S. García-Loyola (2015), Presence of nitrous oxide hotspots in the
1071 coastal upwelling area off central Chile: an analysis of temporal variability based on
1072 ten years of a biogeochemical time series, *Environmental Research Letters*, *10*(4),
1073 044017.
1074 Frame, C., and K. Casciotti (2010), Biogeochemical controls and isotopic signatures of
1075 nitrous oxide production by a marine ammonia-oxidizing bacterium, *Biogeosciences*,
1076 *7*, 2695-2709.
1077 Fuchsman, C. A., A. H. Devol, J. K. Saunders, C. McKay, and G. Rocap (2017), Niche
1078 Partitioning of the N cycling microbial community of an offshore Oxygen Deficient
1079 Zone, *Frontiers in microbiology*, *8*, 2384.
1080 Ganesh, S., D. J. Parris, E. F. DeLong, and F. J. Stewart (2014), Metagenomic analysis of
1081 size-fractionated picoplankton in a marine oxygen minimum zone, *ISME J*, *8*(1), 187-
1082 211.
1083 Ganesh, S., L. A. Bristow, M. Larsen, N. Sarode, B. Thamdrup, and F. J. Stewart (2015),
1084 Size-fraction partitioning of community gene transcription and nitrogen metabolism in
1085 a marine oxygen minimum zone, *The ISME journal*, *9*(12), 2682.
1086 Glibert, P., F. Lipschultz, J. McCarthy, and M. Altabet (1982), Isotope dilution models of
1087 uptake and remineralization of ammonium by marine plankton, *Limnol. Oceanogr.*,
1088 *27*(4), 639-650.

1089 Goreau, T. J., W. A. Kaplan, S. C. Wofsy, M. B. McElroy, F. W. Valois, and S. W. Watson
1090 (1980), Production of NO_2- and N_2O by nitrifying bacteria at reduced concentrations
1091 of oxygen, *Appl. Environ. Microbiol.*, *40*, 526-532.
1092 Granger, J., and S. D. Wankel (2016), Isotopic overprinting of nitrification on denitrification
1093 as a ubiquitous and unifying feature of environmental nitrogen cycling, *Proceedings of*
1094 *the National Academy of Sciences*, *113*(42), E6391-E6400.
1095 Granger, J., D. M. Sigman, M. G. Prokopenko, M. F. Lehmann, and P. D. Tortell (2006), A
1096 method for nitrite removal in nitrate N and O isotope analyses, *Limnology and*
1097 *OceanographyMethods*, *4*(3432), 205-212.
1098 Haskell, W. Z., W. M. Berelson, D. E. Hammond, and D. G. Capone (2013), Particle sinking
1099 dynamics and POC fluxes in the Eastern Tropical South Pacific based on 234Th
1100 budgets and sediment trap deployments, *Deep Sea Res. I*, *81*, 1-13.
1101 Haskell, W. Z., D. Kadko, D. E. Hammond, A. N. Knapp, M. G. Prokopenko, W. M.
1102 Berelson, and D. G. Capone (2015), Upwelling velocity and eddy diffusivity from 7Be
1103 measurements used to compare vertical nutrient flux to export POC flux in the Eastern
1104 Tropical South Pacific, *Mar. Chem.*, *168*, 140-150.
1105 Ho, D. T., C. S. Law, M. J. Smith, P. Schlosser, M. Harvey, and P. Hill (2006), Measurements
1106 of air - sea gas exchange at high wind speeds in the Southern Ocean: Implications for
1107 global parameterizations, *Geophys. Res. Lett.*, *33*(16).
1108 Holmes, R. M., A. Aminot, R. Kèrouel, B. A. Hooker, and B. J. Peterson (1999), A simple
1109 and precise method for measuring ammonium in marine and freshwater ecosystems,
1110 *Canadian Journal of Fisheries and Aquatic Sciences*, *56*(10), 1801-1808.
1111 Horak, R. E., W. Qin, A. D. Bertagnolli, A. Nelson, K. R. Heal, H. Han, M. Heller, A. J.
1112 Schauer, W. H. Jeffrey, and E. V. Armbrust (2018), Relative impacts of light,
1113 temperature, and reactive oxygen on thaumarchaeal ammonia oxidation in the North
1114 Pacific Ocean, *Limnol. Oceanogr.*, *63*(2), 741-757.
1115 Jacob, J., B. Nowka, V. Merten, T. Sanders, E. Spieck, and K. Dähnke (2017), Oxidation
1116 kinetics and inverse isotope effect of marine nitrite-oxidizing isolates, *Aquat. Microb.*
1117 *Ecol.*, *80*(3), 289-300.
1118 Ji, Q. X., A. R. Babbin, A. Jayakumar, S. Oleynik, and B. B. Ward (2015), Nitrous oxide
1119 production by nitrification and denitrification in the Eastern Tropical South Pacific
1120 oxygen minimum zone, *Geophys. Res. Lett.*, *42*(24), 10755-10764.
1121 Ji, Q. X., E. Buitenhuis, P. Suntharalingam, J. L. Sarmiento, and B. B. Ward (2018), Global
1122 Nitrous Oxide Production Determined by Oxygen Sensitivity of Nitrification and
1123 Denitrification, *Global Biogeochemical Cycles*, *32*(12), 1790-1802.
1124 Johnson, M. T., P. S. Liss, T. G. Bell, T. J. Lesworth, A. R. Baker, A. J. Hind, T. D. Jickells,
1125 K. F. Biswas, E. M. S. Woodward, and S. W. Gibb (2008), Field observations of the
1126 ocean-atmosphere exchange of ammonia: Fundamental importance of temperature as
1127 revealed by a comparison of high and low latitudes, *Global Biogeochemical Cycles*,
1128 *22*(1).
1129 Jung, M.-Y., J.-H. Gwak, L. Rohe, A. Giesemann, J.-G. Kim, R. Well, E. L. Madsen, C. W.
1130 Herbold, M. Wagner, and S.-K. Rhee (2019), Indications for enzymatic denitrification
1131 to N 2 O at low pH in an ammonia-oxidizing archaeon, *The ISME journal*, 1.
1132 Kalvelage, T., G. Lavik, P. Lam, S. Contreras, L. Arteaga, C. R. Löscher, A. Oschlies, A.
1133 Paulmier, L. Stramma, and M. M. Kuypers (2013), Nitrogen cycling driven by organic
1134 matter export in the South Pacific oxygen minimum zone, *Nat Geosci*, *6*(3), 228.

Kitzinger, K., H. K. Marchant, L. A. Bristow, C. W. Herbold, C. C. Padilla, A. T. Kidane, S. Littmann, H. Daims, P. Pjevac, and F. J. Stewart (2020), Single cell analyses reveal contrasting life strategies of the two main nitrifiers in the ocean, *Nature communications*, *11*(1), 1-12.

Knapp, A. N., K. L. Casciotti, W. M. Berelson, M. G. Prokopenko, and D. G. Capone (2016), Low rates of nitrogen fixation in eastern tropical South Pacific surface waters, *Proceedings of the National Academy of Sciences*, *113*(16), 4398-4403.

Kozlowski, J. A., M. Stieglmeier, C. Schleper, M. G. Klotz, and L. Y. Stein (2016), Pathways and key intermediates required for obligate aerobic ammonia-dependent chemolithotrophy in bacteria and Thaumarchaeota, *ISME J*, *10*(8), 1836-1845.

Lam, P., M. M. Jensen, G. Lavik, D. F. McGinnis, B. Muller, C. J. Schubert, R. Amann, B. Thamdrup, and M. M. M. Kuypers (2007), Linking crenarchaeal and bacterial nitrification to anammox in the Black Sea, *Proc. Natl. Acad. Sci. U. S. A.*, *104*(17), 7104-7109.

Lam, P., G. Lavik, M. M. Jensen, J. van de Vossenberg, M. Schmid, D. Woebken, D. GutiÈrrez, R. Amann, M. S. M. Jetten, and M. M. M. Kuypers (2009), Revising the nitrogen cycle in the Peruvian oxygen minimum zone, *Proceedings of the National Academy of Sciences*, *106*(12), 4752.

Lipschultz, F., S. C. Wofsy, B. B. Ward, L. A. Codispoti, G. E. Friederich, and J. W. Elkins (1990), Bacterial transformations of inorganic nitrogen in the oxygen-deficient waters of the Eastern Tropical South Pacific Ocean, *Deep Sea Research*, *37*(10), 1513-1541.

Liu, S., P. Han, L. Hink, J. I. Prosser, M. Wagner, and N. Brüggemann (2017), Abiotic conversion of extracellular NH2OH contributes to N2O emission during ammonia oxidation, *Environ. Sci. Technol.*, *51*(22), 13122-13132.

Lomas, M. W., and F. Lipschultz (2006), Forming the primary nitrite maximum: Nitrifiers or phytoplankton?, *Limnol. Oceanogr.*, *51*(5), 2453-2467.

Löscher, C., A. Kock, M. Koenneke, J. LaRoche, H. Bange, and R. Schmitz-Streit (2012), Production of oceanic nitrous oxide by ammonia-oxidizing archaea, *Biogeosciences*, *9*, 2419-2429.

Martin, J. H., G. A. Knauer, D. M. Karl, and W. W. Broenkow (1987), Vertex - Carbon Cycling in the Northeast Pacific, *Deep Sea Res. I*, *34*(2), 267-285.

Martinez-Rey, J., L. Bopp, M. Gehlen, A. Tagliabue, and N. Gruber (2015), Projections of oceanic N2O emissions in the 21st century using the IPSL Earth system model, *Biogeosciences (BG)*, *12*(13), 4133-4148.

McIlvin, M. R., and M. A. Altabet (2005), Chemical conversion of nitrate and nitrite to nitrous oxide for nitrogen and oxygen isotopic analysis in freshwater and seawater, *Anal. Chem.*, *77*(17), 5589-5595.

McIlvin, M. R., and K. L. Casciotti (2010), Fully automated system for stable isotopic analysis of dissolved nitrous oxide at natural abundance levels, *Limnology and Oceanography Methods*, *8*, 54-66.

McIlvin, M. R., and K. L. Casciotti (2011), Technical updates to the bacterial method for nitrate isotopic analyses, *Anal. Chem.*, *83*(5), 1850-1856.

Mincer, T. J., M. J. Church, L. T. Taylor, C. Preston, D. M. Karl, and E. F. DeLong (2007), Quantitative distribution of presumptive archaeal and bacterial nitrifiers in Monterey Bay and the North Pacific Subtropical Gyre, *Environ. Microbiol.*, *9*(5), 1162-1175.

Mosier, A. C., and C. A. Francis (2011), Determining the distribution of marine and coastal ammonia-oxidizing archaea and bacteria using a quantitative approach, *Methods Enzymol.*, *486*, 205-221.
Nevison, C., J. H. Butler, and J. Elkins (2003), Global distribution of N2O and the DN2O-AOU yield in the subsurface ocean, *Global Biogeochem. Cycles*, *17*(4), 1119.
Nevison, C. D., R. F. Weiss, and D. J. Erickson III (1995), Global oceanic emissions of nitrous oxide, *Journal of Geophysical Research: Oceans*, *100*(C8), 15809-15820.
Newell, S. E., A. R. Babbin, A. Jayakumar, and B. B. Ward (2011), Ammonia oxidation rates and nitrification in the Arabian Sea, *Global Biogeochemical Cycles*, *25*, Gb4016.
Owens, S., S. Pike, and K. Buesseler (2015), Thorium-234 as a tracer of particle dynamics and upper ocean export in the Atlantic Ocean, *Deep Sea Res. II*, *116*, 42-59.
Paulot, F., D. J. Jacob, M. T. Johnson, T. G. Bell, A. R. Baker, W. C. Keene, I. D. Lima, S. C. Doney, and C. A. Stock (2015), Global oceanic emission of ammonia: Constraints from seawater and atmospheric observations, *Global Biogeochemical Cycles*, *29*(8), 1165-1178.
Peng, X., C. A. Fuchsman, A. Jayakumar, S. Oleynik, W. Martens - Habbena, A. H. Devol, and B. B. Ward (2015), Ammonia and nitrite oxidation in the Eastern Tropical North Pacific, *Global Biogeochemical Cycles*, *29*(12), 2034-2049.
Peng, X. F., C. A. Fuchsman, A. Jayakumar, M. J. Warner, A. H. Devol, and B. B. Ward (2016), Revisiting nitrification in the Eastern Tropical South Pacific: A focus on controls, *J. Geophys. Res.*, *121*(3), 1667-1684.
Ploug, H., and J. Bergkvist (2015), Oxygen diffusion limitation and ammonium production within sinking diatom aggregates under hypoxic and anoxic conditions, *Mar. Chem.*, *176*, 142-149.
Prairie, J. C., K. Ziervogel, R. Camassa, R. M. McLaughlin, B. L. White, Z. I. Johnson, and C. Arnosti (2017), Ephemeral aggregate layers in the water column leave lasting footprints in the carbon cycle, *Limnology and Oceanography Letters*, *2*(6), 202-209.
Qin, W., K. A. Meinhardt, J. W. Moffett, A. H. Devol, E. V. Armbrust, A. E. Ingalls, and D. A. Stahl (2017), Influence of oxygen availability on the activities of ammonia-oxidizing archaea, *Environmental Microbiology Reports*, *9*(3), 250-256.
Raimbault, P., N. Garcia, and F. Cerutti (2008), Distribution of inorganic and organic nutrients in the South Pacific Ocean-evidence for long-term accumulation of organic matter in nitrogen-depleted waters, *Biogeosciences*, *5*(2), 281-298.
Santoro, A. E., K. L. Casciotti, and C. A. Francis (2010), Activity, abundance and diversity of nitrifying archaea and bacteria in the central California Current, *Environ. Microbiol.*, *12*, 1989-2006.
Santoro, A. E., C. Buchwald, M. R. McIlvin, and K. L. Casciotti (2011), Isotopic composition of N2O produced by marine ammonia-oxidizing archaea, *Science*, *333*, 1282.
Santoro, A. E., M. A. Saito, T. J. Goepfert, C. H. Lamborg, C. L. Dupont, and G. R. DiTullio (2017), Thaumarchaeal ecotype distributions across the equatorial Pacific Ocean and their potential roles in nitrification and sinking flux attenuation, *Limnol. Oceanogr.*, *62*(5), 1984-2003.
Santoro, A. E., C. M. Sakamoto, J. M. Smith, J. N. Plant, A. L. Gehman, A. Z. Worden, K. S. Johnson, C. A. Francis, and K. L. Casciotti (2013), Measurements of nitrite production in and around the primary nitrite maximum in the central California Current, *Biogeosciences*, *10*(11), 7395-7410.

Santoro, A. E., C. L. Dupont, R. A. Richter, M. T. Craig, P. Carini, M. R. McIlvin, Y. Yang, W. D. Orsi, D. M. Moran, and M. A. Saito (2015), Genomic and proteomic characterization of "Candidatus Nitrosopelagicus brevis": An ammonia-oxidizing archaeon from the open ocean, *Proc. Natl. Acad. Sci. U. S. A.*, *112*(4), 1173-1178.

Sigman, D. M., K. L. Casciotti, M. Andreani, C. Barford, M. Galanter, and J. K. Bohlke (2001), A bacterial method for the nitrogen isotopic analysis of nitrate in seawater and freshwater, *Anal. Chem.*, *73*(17), 4145-4153.

Sigman, D. M., J. Granger, P. J. DiFiore, M. F. Lehmann, R. Ho, G. Cane, and A. van Geen (2005), Coupled nitrogen and oxygen isotope measurements of nitrate along the eastern North Pacific margin, *Global Biogeochem. Cycles*, *19*(4), GB4022.

Smith, J. M., F. P. Chavez, and C. A. Francis (2014a), Ammonium uptake by phytoplankton regulates nitrification in the sunlit ocean, *Plos One*, *9*(9), e108173.

Smith, J. M., K. L. Casciotti, F. P. Chavez, and C. A. Francis (2014b), Differential contributions of archaeal ammonia oxidizer ecotypes to nitrification in coastal surface waters, *ISME J*, *8*(8), 1704-1714.

Smith, J. M., J. Damasheck, F. P. Chavez, and C. A. Francis (2015), Factors influencing nitrification rates and the abundance and transcriptional activity of ammonia-oxidizing microorganisms in the dark northeast Pacific Ocean, *Limnol. Oceanogr.*

Stieglmeier, M., M. Mooshammer, B. Kitzler, W. Wanek, S. Zechmeister-Boltenstern, A. Richter, and C. Schleper (2014), Aerobic nitrous oxide production through N-nitrosating hybrid formation in ammonia-oxidizing archaea, *ISME J*, *8*(5), 1135-1146.

Strickland, J., and T. Parsons (1968), A practical handbook of seawater analysis, *Fisheries Research Board of Canada Bulletin*, *167*, 71-75.

Sun, X., L. F. Kop, M. C. Lau, J. Frank, A. Jayakumar, S. Lücker, and B. B. Ward (2019), Uncultured Nitrospina-like species are major nitrite oxidizing bacteria in oxygen minimum zones, *The ISME journal*, *13*(10), 2391-2402.

Suntharalingam, P., J. Sarmiento, and J. Toggweiler (2000), Global significance of nitrous-oxide production and transport from oceanic low-oxygen zones: A modeling study, *Global Biogeochemical Cycles*, *14*(4), 1353-1370.

Taylor, B. W., C. F. Keep, R. O. Hall, B. J. Koch, L. M. Tronstad, A. S. Flecker, and A. J. Ulseth (2007), Improving the fluorometric ammonium method: matrix effects, background fluorescence, and standard additions, *J N Am Benthol Soc*, *26*(2), 167-177.

Trimmer, M., P. M. Chronopoulou, S. T. Maanoja, R. C. Upstill-Goddard, V. Kitidis, and K. J. Purdy (2016), Nitrous oxide as a function of oxygen and archaeal gene abundance in the North Pacific, *Nature Communications*, *7*.

Wanninkhof, R. (1992), Relationship between wind speed and gas exchange, *J. Geophys. Res*, *97*(25), 7373-7382.

Ward, B., A. Devol, J. Rich, B. Chang, S. Bulow, H. Naik, A. Pratihary, and A. Jayakumar (2009), Denitrification as the dominant nitrogen loss process in the Arabian Sea, *Nature*, *461*(7260), 78-81.

Ward, B. B. (2008), Nitrification in Marine Systems, in *Nitrogen in the Marine Environment*, edited by D. G. Capone, D. A. Bronk, M. R. Mulholland and E. J. Carpenter, pp. 199-262, Elsevier.

Ward, B. B., and O. C. Zafiriou (1988), Nitrification and nitric oxide in the oxygen minimum of the eastern tropical North Pacific, *Deep Sea Res. I*, *35*(7), 1127-1142.

Ward, B. B., H. E. Glover, and F. Lipschultz (1989), Chemoautotrophic activity and nitrification in the oxygen minimum zone off Peru, *Deep Sea Res. I*, *36*(7), 1031-1051.

Winkler, M.-K., Q. H. Le, and E. I. Volcke (2015), Influence of partial denitrification and mixotrophic growth of NOB on microbial distribution in aerobic granular sludge, *Environ. Sci. Technol.*, *49*(18), 11003-11010.

Wuchter, C., et al. (2006), Archaeal nitrification in the ocean, *Proc. Natl. Acad. Sci. U. S. A.*, *103*(33), 12317-12322.

Yang, S., et al. (in press), Global reconstruction reduces the uncertainty of oceanic nitrous oxide emissions and reveals a vigourus seasonal cycle, *Proceedings of the National Academy of Sciences*.

Yeung, L. Y., W. M. Berelson, D. E. Hammond, M. G. Prokopenko, C. Wolfe, and N. Rollins (2015), Upper-ocean gas dynamics from radon profiles in the Eastern Tropical South Pacific, *Deep Sea Res. I*, *99*, 35-45.

Yoshida, N., H. Morimoto, M. Hirano, I. Koike, S. Matsuo, E. Wada, T. Saino, and A. Hattori (1989), Nitrification rates and 15N abundances of N2O and NO3- in the western North Pacific, *Nature*, *342*, 895-897.

Zafiriou, O. C., and M. B. True (1979), Nitrate photolysis in seawater by sunlight, *Mar. Chem.*, *8*(1), 33-42.

Zakem, E. J., A. Al-Haj, M. J. Church, G. L. Dijken, S. Dutkiewicz, S. Q. Foster, R. W. Fulweiler, M. M. Mills, and M. J. Follows (2018), Ecological control of nitrite in the upper ocean, *Nature communications*, *9*(1), 1206.

Zamora, L., A. Oschlies, H. Bange, K. Huebert, J. Craig, A. Kock, and C. Löscher (2012), Nitrous oxide dynamics in low oxygen regions of the Pacific: insights from the MEMENTO database, *Biogeosciences*, *9*(12), 5007-5022.